END

FILMED

DTIC

MICROCOPY RESOLUTION TEST CHART
NATIONAL BUREAU OF STANDARDS-1963-A

SECURITY CLASSIFICATION OF THIS PAGE

REPORT DOCUMENTATION PAGE

1a. R U	1b. RESTRICTIVE MARKINGS
2a. SI **AD-A158 872** 2b. D	3. DISTRIBUTION/AVAILABILITY OF REPORT Unclassified; distribution unlimited
4. PERFORMING ORGANIZATION REPORT NUMBER(S) Technical Report #114	5. MONITORING ORGANIZATION REPORT NUMBER(S)

6a. NAME OF PERFORMING ORGANIZATION	6b. OFFICE SYMBOL (If applicable)	7a. NAME OF MONITORING ORGANIZATION
University of Michigan		Physics Division Office of Naval Research

6c. ADDRESS (City, State and ZIP Code)	7b. ADDRESS (City, State and ZIP Code)
University of Michigan Ann Arbor, MI 48109	800 N. Quincy St. Arlington, VA 22217

8a. NAME OF FUNDING/SPONSORING ORGANIZATION	8b. OFFICE SYMBOL (If applicable)	9. PROCUREMENT INSTRUMENT IDENTIFICATION NUMBER
Office of Naval Research		

8c. ADDRESS (City, State and ZIP Code)	10. SOURCE OF FUNDING NOS.			
800 N. Quincy Street Arlington, VA 22217	PROGRAM ELEMENT NO.	PROJECT NO. N00014 81K 0700	TASK NO.	WORK UNIT NO.

11. TITLE (Include Security Classification)
Investigations of Laser Initiated Discharge Channels

12. PERSONAL AUTHOR(S)
R. M. Gilgenbach & T. Kammash

13a. TYPE OF REPORT	13b. TIME COVERED	14. DATE OF REPORT (Yr., Mo., Day)	15. PAGE COUNT
Annual Summary	FROM 10/85 TO 8/85	8/19/85	

16. SUPPLEMENTARY NOTATION

SEP 1 0 1985

17. COSATI CODES			18. SUBJECT TERMS (Continue on reverse if necessary and identify by block number)
FIELD	GROUP	SUB. GR.	Channels, laserguided discharges

A

19. ABSTRACT (Continue on reverse if necessary and identify by block number)

We report progress on the generation of intense, microsecond, electron beams. Diode closure has been studied for electron beam pulselengths up to 4 microseconds.

Reduced density channels produced by laser induced gas breakdown and by laser guided discharges are modelled by means of a one dimensional gas hydrodynamics code for times earlier than the onset of convective mixing. Comparison of laser induced gas breakdown experiments with the code indicate that the conversion of laser energy to gas heating is limited to 25-30%. Collinear
(cont.)

DTIC FILE COPY

20. DISTRIBUTION/AVAILABILITY OF ABSTRACT	21. ABSTRACT SECURITY CLASSIFICATION
UNCLASSIFIED/UNLIMITED ☒ SAME AS RPT ☐ DTIC USERS ☐	UNCLASSIFIED

22a. NAME OF RESPONSIBLE INDIVIDUAL	22b. TELEPHONE NUMBER (Include Area Code)	22c. OFFICE SYMBOL
C. W. Roberson	(202) 696-4222	

DD FORM 1473, 83 APR   EDITION OF 1 JAN 73 IS OBSOLETE   UNCLASSIFIED

holographic measurements of channel density profiles produced by laser guided discharges are found to be in good agreement with code predictions for times less than 50 s. This agrees with other experiments which have indicated onset times for convective mixing in the range 50-70 μs after the start of the discharge.

A Monte Carlo Fokker Planck code is used to investigate the scattering loss of particles from a relativistic electron beam propagating in a low pressure air channel. The fraction of particles transmitted is calculated and its variation with relevant beam and channel parameters is obtained. The effect of multiple scattering is examined, and a parameter reflecting scattering erosion rate is calculated for some experimentally observed parameters and found to agree with an analytical expression for force-free propagation.

Accession For

NTIS CRA&I

DTIC TAB

Unannounced

Justification

By

Distribution/

Availability Codes

Dist   Avail and/or Special

A-1

Ŕ. M. Gilgenbach and T. Kammash, Nuclear Engineering Dept., U. of Mich.

Appendix I

During the past year we have made significant progress
in the generation of multimicrosecond electron beams on
MELBA. In a recent invited talk at the IEEE Pulse Power
Conference we reported generation of 4 microsecond electron
beams, believed to be the longest intense beam pulselengths
in the U. S. In these experiments we discovered significant
effects of anode conditions upon electron beam diode
impedance. These results are fully described in the attached
reprint from the conference proceedings.

In the area of shock wave generation, diagnosis and
modeling, we have successfully employed a 1-dimensional
hydrodynamics code to estimate the energy deposition in
channels by lasers and guided discharges. The collinear
holographic intreferometry results have been previously
published and the comparison of data to the code is given in
the doctoral dissertation of L. D. Horton, summarized in the
attached technical report.

Initial electron beam interaction experiments have
concentrated on the interaction of 0.4 microsecond Febetron
beams with argon and nitrogen. These results were presented
at the 1984 APS-DPP meeting. Some of the significant
findings are shown in Figures I-1, I-2, I-3, and I-4. These
figures give as a function of pressure, the transmitted
current to a bare collector located 0.85 m from the entrance
foil. Also shown are the collector current decay times for
these cases. It can be seen that, for the 1 kA injected

current, less than 50% is measured by the collector. Another interesting feature was that the collector current decay time was larger in argon than nitrogen indicating that the L/R time for argon is longer (giving a lower R) for the postbeam channel.

In the area of diagnostics we have investigated several new configurations including:

1) a single optical fiber probe to measure spatial and temporal electron beam profiles within a plasma, and

2) Lucite plate diagnostics for measurement of electron beam uniformity and potentially emittance in the diode.

The abstract from a paper describing these diagnostics is attached. Data from the fiberoptic probe is presented in Fig. I-3.

Most of the effort for the past year was devoted to improving the Monte Carlo Fokker-Planck Code to incorporate the self field of the beam. This is in its last stage and in the near future the code will be tested on known cases to assess the role of the self field on the scattering losses from an intense relativistic electron beam propagating in a low pressure laser-initiated channel.

In the course of that study the code without the self field was also tested by investigating the erosion of an electron beam propagating in the ion focused regime as generated by the ETA experiment. Since there are several mechanisms responsible for beam erosion the usefulness of this code was employed to estimate the scattering effects. The effects of multiple scattering were also addressed and their variation with such parameters as beam

85 9 09 151

density, channel neutral and electron densities, and beam and channel radii. The results of this study are summarized in a paper published in the 1984 proceedings of the Annual propagation meeting (copy attached) and in a paper presented at the annual APS plasma physics meeting.
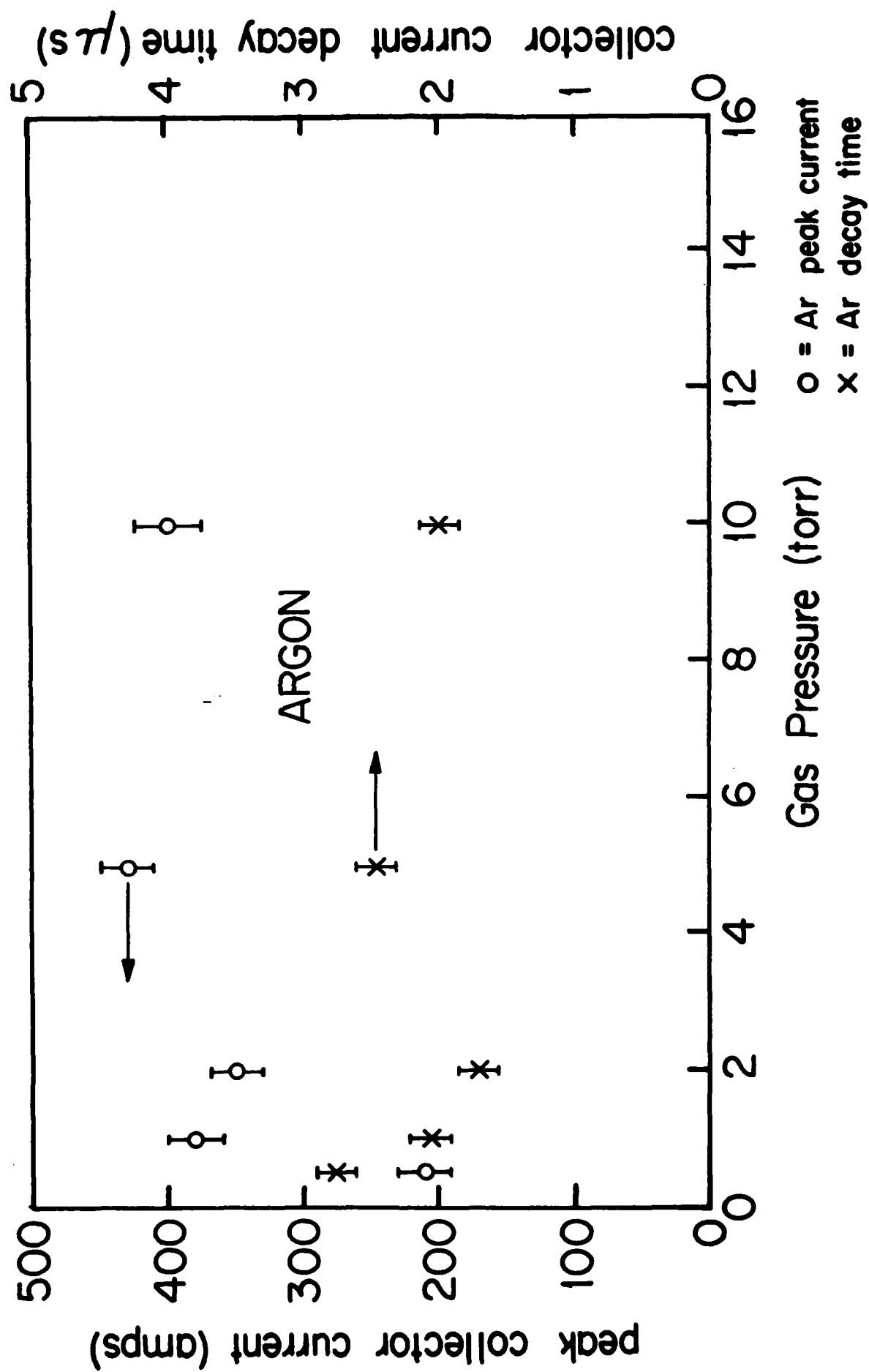
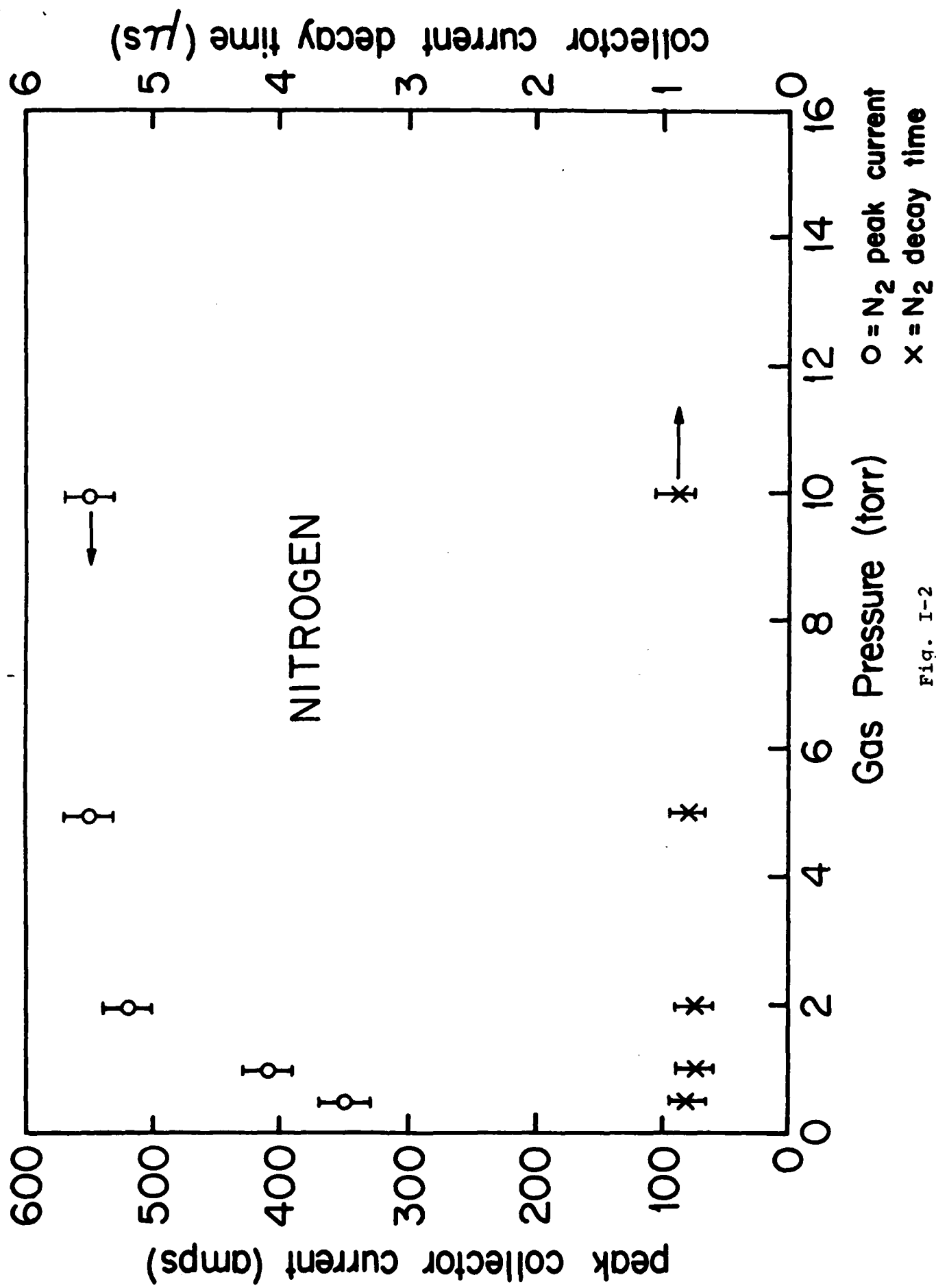collector current decay time (μs)

peak collector current (amps)

Gas Pressure (torr)

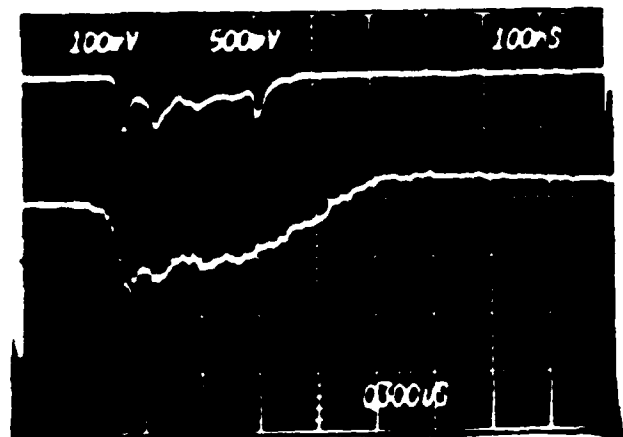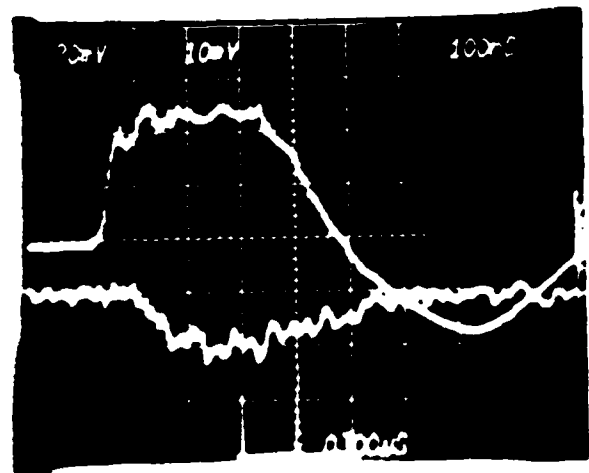o = Ar peak current
x = Ar decay time

ARGON

Fig. I-1

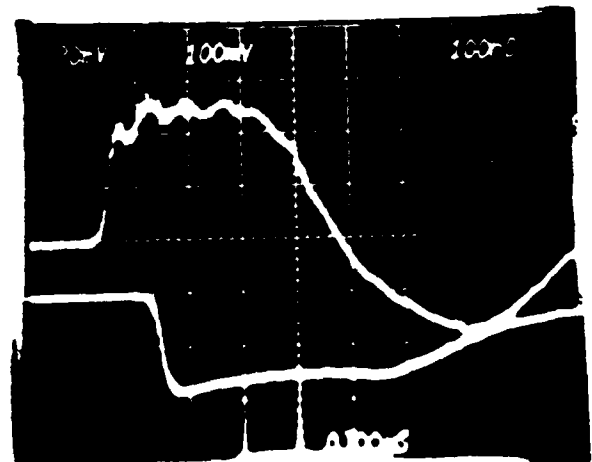Fig. I-2

FEBETRON ELECTRON BEAM DATA

CATHODE VOLTAGE
(PEAK OF ABOUT 300 kV)

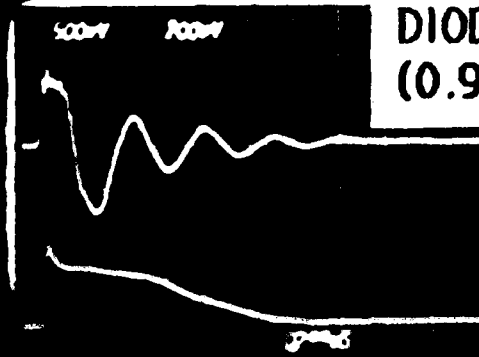DIODE ELECTRON BEAM CURRENT
(0.4 kA/DIV)

BEAM X-RAY SIGNAL

PLASMA LIGHT SIGNAL

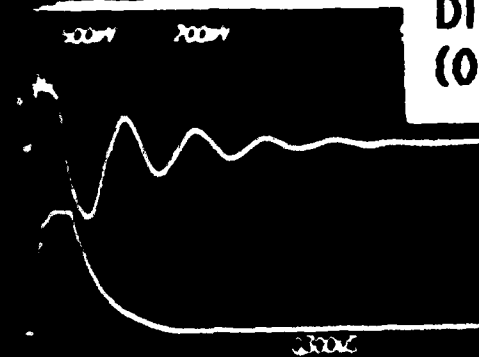Fig. I-3

CURRENT SUSTAINMENT DATA
(0.5 MICROSEC./DIV)

ARGON DATA (2 TORR)

**DIODE E-BEAM CURRENT
(0.9 kA/DIV)**

**COLLECTOR CURRENT
(0.4 kA/DIV)**

NITROGEN DATA (2 TORR)

**DIODE E-BEAM CURRENT
(0.9 kA/DIV)**

**COLLECTOR CURRENT
(0.4 kA/DIV)**

COMPARISON OF THE L/R DECAY TIMES FOR
THE TWO GASES INDICATE THAT THE
POST-BEAM RESIDUAL RESISTIVITY OF
NITROGEN PLASMA CHANNELS IS AT LEAST A

FACTOR OF TWO HIGHER THAN FOR ARGON

Appendix II

   Publications and Papers Sponsored by this Contract

Invited Paper: "Microsecond Electron Beam Diode Closure
Experiments," R. M. Gilgenbach et al, Submitted to 4th IEEE
Pulsed Power Conference, June 10-12, 1985, Arlington, VA.

"Microsecond Electron Beam Interactions with Monatomic and
Diatomic Gases," with L. D. Horton, M. L. Brake, R. F. Lucey,
and J. E. Tucker. Presented at the 26th Annual Meeting of
the Division of Plasma Physics of the American Physical
Society, Oct. 29 to Nov. 2, 1984, Boston, MA.

"Hydrodynamics of Gas Channels Formed by Lasers and Guided
Discharges," Doctoral Dissertation by L. D. Horton.

"Gas Hydrodynamics of Channels Formed by Lasers and Laser
Guided Discharges," L. D. Horton and R. M. Gilgenbach,
Submitted to the 1985 IEEE International Conference on
Plasma Science, June 3-5, 1985, Pittsburgh, PA.

"Spatially and Temporally Resolved Detection of a
Relativistic Electron Beam Streaming Through a Plasma
Background," R. M. Gilgenbach, L. D. Horton, S. Bidwell, R.
F. Lucey, L. Smutek, and J. E. Tucker, Technical Report in
preparation.

"Beam Erosion Due to Scattering in Low Pressure Media,"
Proc. Annual Propagation Meeting, July 1984, Monterey.

"Multiple Scattering Losses of Charged Particle Beams in
Low-Pressure Gasses," Bull. Am. Phy. Soc. 29, 1274 (1984).

19

Appendix III

Personnel Receiving Partial Support from This Project

Co-Principal Investigators: R. M. Gilgenbach and T. Kammash

Graduate Students: R. F. Lucey, Jr., L. D. Horton, J. Miller, and J. Les

L. D. Horton received his Ph.D. and will be starting a position as a NATO Postdoctoral Fellow at Culham Laboratory in September.

Appendix IV

Reprints of Publications Supported by This Contract

MICROSECOND ELECTRON BEAM DIODE CLOSURE EXPERIMENTS *

R. M. Gilgenbach, L. D. Horton, R. F. Lucey, Jr,
S. Bidwell, M. Cuneo, J. Miller, and L. Smutek

Intense Energy Beam Interaction Laboratory
Nuclear Engineering Department
The University of Michigan
Ann Arbor, Michigan 48109

Abstract

Experiments have been conducted on the
Michigan Electron Long Beam Accelerator
(MELBA) to explore diode closure and voltage
compensation during collapsing diode
impedance. MELBA operates with parameters:
Voltage = - 0.6 to -1.0 MV; Current < 60 kA;
and Pulselengths exceeding 1 µs. A reverse
charged ringing circuit compensates the Marx
generator output voltage to within ± 7 %
(± 10%) for pulselengths of 1 µs (1.4 µs) in
a 127 ohm resistive load. Electron beam
generation experiments have utilized two
types of field emission cathodes: carbon
brush and velvet cloth. Total electron beam
pulselengths of 4 µs have been achieved.
Voltage compensation is limited by current
spikes to ±13% (±5%) over the first
1 µs (0.7 µs). Diode impedance and perveance
have been characterized as a function of time
at several A-K gap spacings. Current
densities have been in the range from 10 to
200 A/cm^2. The current shows an initial
step with a rapid increase at 0.6 to 0.8 µs
followed by either current runaway or a
return to Child-Langmuir. Apertured electron
beam current shows a similar behavior with
large amplitude beam fluctuations during
enhanced current. Apparent plasma closure
velocities inferred from diode impedance
data indicate closure velocities from 3.3 to
6.2 cm/µs dependent upon the cathode type.
The effective closure velocity, defined by
the time required to short circuit the A-K
gap, ranges from 2.1 to 4.1 cm/µs. Electron
beam uniformity and beam dynamics have been
investigated by means of apertured anodes
with lucite plate diagnostics. Voltage
compensation has been tested by comparing
experimental voltage traces to transient
circuit computer codes with empirical
impedance profiles.

Introduction

Most research concerning intense, pulsed
electron beams has utilized pulselengths in
the range from tens to hundreds of ns. This
was due in part to specific applications,
(such as inertial confinement fusion), which
require short, intense, pulses of energy.

Accelerator size and cost can be reduced
when large delivered energies are generated
by increasing the beam pulselength rather
than the voltage and current. Earlier
experiments [1-8] have generated intense,
microsecond electron beams by means of Marx
generators with pulse forming lines (PFL) or
pulse forming networks (PFN). In this article
we demonstrate microsecond electron beam
generation and voltage compensation with a
Marx generator coupled to an Abramyan type
RLC ringing, reverse-charged stage [9, 10].

The advantages of the Abramyan circuit
over Marx generators with PFLs or PFNs are:
1) It requires fewer circuit elements, thus
   providing more compact, less expensive
   generators,
2) Compensation for different load
   impedances can be changed by adjusting the
   relative charging voltages rather than by
   changing PFN circuit elements,
3) The Marx generator directly drives the
   load, so the voltage requirement is
   lowered.

Intense electron beams with pulselengths
exceeding 1 µs have a number of important
applications:
1) Pumping of lasers in the visible, uv, and
   (possibly) X-ray regime [4,10],
2) High power microwave and millimeter wave
   generators and free electron lasers [11],
3) Fusion plasma startup, heating,
   and stabilization,
4) Pulsed X-ray radiography, and
5) Rapid heating of materials and gases.

Each of these applications imposes different
constraints on the cathode current density
and voltage flatness. Electron beam pumped
lasers might require a current density on
the order of 30 A/cm^2, whereas high power
microwave generators operating in the
collective regime may need kA/cm^2.

Explosive emission cathodes [1-16] have
generally been employed in these applications
because of their high current densities and
immunity to the hostile plasma chemistry en-
vironment which poisons thermionic cathodes.
This presents a problem in the generation of
microsecond electron beams because of the
rapid closure of the anode-cathode (A-K) gap
by the cathode plasma. According to the
Child-Langmuir current scaling, this gap
closure causes an increase in the electron
current density by the factor $(d - ut)^{-2}$;
where d is the initial A-K gap spacing and
u is the closure velocity. Another problem
intricately related to this increasing
current is the maintainance of a flat output
voltage throughout the µs pulse. Constancy
of the beam voltage is particularly important
for microwave generators which must satisfy
resonance conditions. The plasma closure
velocity is therefore crucial in determining
diode impedance collapse, voltage droop, and
A-K gap shorting.

MELBA Design and Performance

The Michigan Electron Long Beam Acceler-
ator (MELBA) was designed [17] to generate
10 kA, 1 MV electron beams into a collapsing
diode impedance for 1 µs pulselengths. The
design utilizes an electrical voltage compen-
sation circuit first proposed by Abramyan [9]
and later by Smith [10]. This circuit

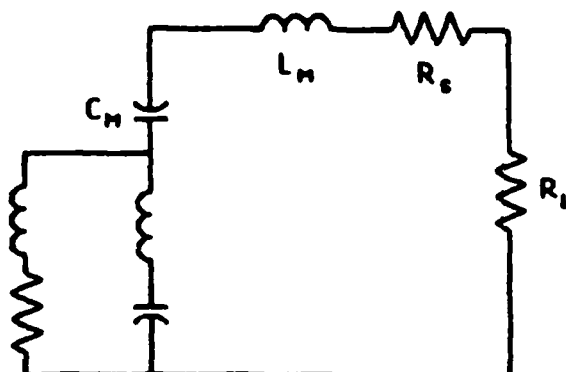employs a Marx generator coupled to a ringing
RLC circuit.

Fig. 1. Simplified schematic of the
Abramyan circuit with all spark gap
switches closed [9,10]. Not shown
are the Marx/switch resistances.

The MELBA design also includes a small RC
filter circuit on the output. The ringing
stage (RS) is charged to initially deliver
a voltage of the opposite polarity from the
Marx output. At a later time, the polarity
of the RS is in the same sense as the Marx
output. Separate charging supplies are
utilized for the Marx generator and the
ringing stage. This allows the amount of
voltage compensation to be changed by choos-
ing the relative charging voltage of the Marx
versus the ringing stage. The spark gap
switches in the Marx generator and the RS are
independently triggered; in these experiments
the two circuits were triggered simultan-
eously. MELBA utilizes 14 capacitors in the
Marx generator and 2 capacitors in the RS,
one third the number of capacitors used in
other microsecond electron beam generators
[2,3].

Data in Fig. 2 represent a -1 MV out-
put voltage from the MELBA machine into a low
inductance 127 ohm resistive load; also shown
is the output of the SPICE transient circuit
analysis code [18] to illustrate the effect
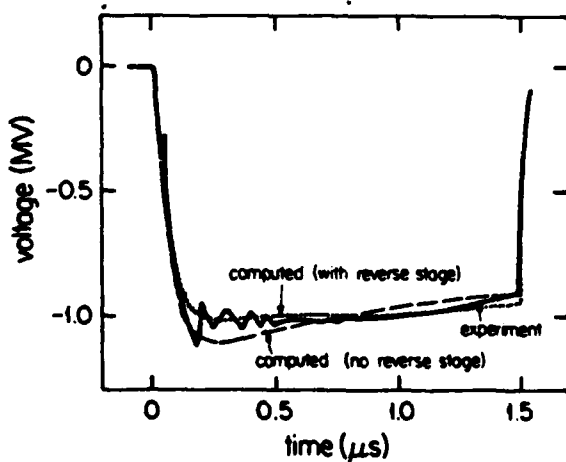of the ringing, reverse-charged stage.

Fig. 2. MELBA output voltage into 127 ohm
resistive load.

From the above data it can be seen that the
experimental voltage remains flat to within
± 7 % (±10 %) over pulselengths of 1 μs
(1.4 μs). The transient circuit code gives
excellent agreement with experimental data.
It should also be noted from the computer
model that without the ringing stage, the
voltage would not be flat but would exhibit
the RC decay characteristic of Marx
rundown circuits.

The generator was constructed with a
triggered, high pressure SF₆ crowbar switch
to short circuit the generator output after
the design pulselength of 1 μs. The crowbar
switch removed 90% of the generator voltage
in about 40 ns. Figure 3 gives the output
voltage and current into a resistive load
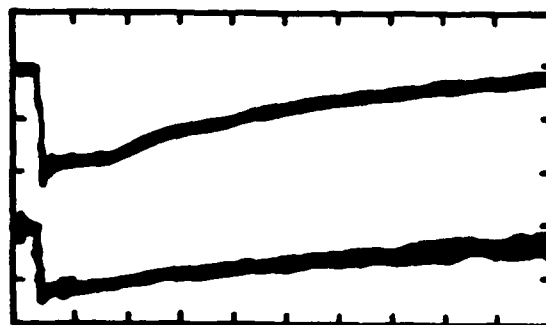without crowbar firing.

Fig. 3. Voltage (upper, 400 kV/div) and cur-
rent (lower) into 127 ohm resistive
load without crowbar firing
- (1μs/div). Charging voltages:
V_M = ± 56 kV; V_r = ± 54 kV.

The data of Fig. 3 demonstrate the
effectiveness of the RS in generating flat
voltage out to 1.4 μs. The fact that
voltage remains on the load for about
10 μs into a resistive load is important for
comparison with the electron beam diode
closure experiments. The resistor in series
with the cathode (Fig. 1) dissipates the
stored generator energy in the event of a
crowbar or A-K short circuit. This feature
permitted experiments to be performed without
firing the crowbar in order to investigate
plasma closure and shorting with multimicro-
second pulselengths.

Cathode - Anode Configuration

The anode-cathode geometry is depicted
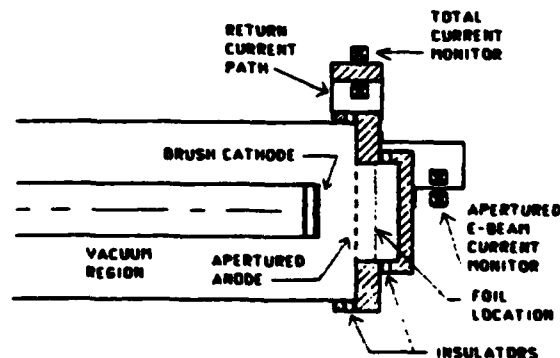in Fig. 4.

Fig. 4. Anode-cathode configuration.

Since the objective of these experiments was to investigate high current electron beams with multimicrosecond pulselengths, the anode-cathode spacings were relatively large: 10 cm for most shots, although 8 cm and 6 cm were also used. In order to extract multikiloampere currents, two types of large area field emission cathodes were employed in these experiments:
1) carbon brush cathode, and
2) velvet cloth cathode.

The brush cathode was constructed following the design of Refs. 4 and 11. Carbon string was threaded through a square array of holes on 1 cm centers in a 7 cm radius aluminum plate. The outer radius of the carbon brush array was 6 cm. A smaller (2.5 cm radius) brush cathode was also constructed with recessed CR-39 ion track film to detect ions crossing the A-K gap.

The velvet cathode used in these experiments was 65 % cotton and 35 % rayon. A 6 cm radius circle of this cloth was epoxied to a 7 cm radius aluminum cathode plate.

In both cases, the cathode plate was threaded to the anodized cathode stalk of radius 7 cm. Anode-cathode spacings were adjusted by installing anodized rings between the cathode stalk and the cathode plate.

An extremely durable anode design was required, since the generator was typically operated in a noncrowbarred mode in which plasma shorting of the A-K gap occurred. For this reason it was not possible for foil anodes (or even solid molybdenum anodes) to survive the high current discharge from the capacitor bank after A-K shorting. The high current discharge was much more damaging to anode materials because high current densities deposit energy at the surface, removing material in a vacuum arc mechanism [19]. It was found that a (3.2 mm thick) Poco-graphite anode produced the least contamination of the cathode and insulators for shorted A-K gaps.

The anode plate was insulated from the vacuum tank and up to 6 current transformers were utilized to monitor total return current which passed through low inductance straps. Current signals were summed in the Faraday cage by ferrite adders. Electron beam current was sampled by an array of small (1.6 mm) holes in the graphite anode plate. A beam collector and current transformer permitted measurements of apertured electron beam current. Energy discrimination of apertured electron beam current could be performed by installing foil between the carbon anode and the beam collector. For studies of electron beam uniformity and beam dynamics the electron beam collector was replaced by a lucite plate. The inside of this plate was coated by an opaque layer of Aerodag graphite spray; the outside of this plate was viewed by either an open shutter or streak camera.

Electron Beam Generation Experiments

Brush cathode turn-on data is presented in the voltage and current traces of Figure 5.
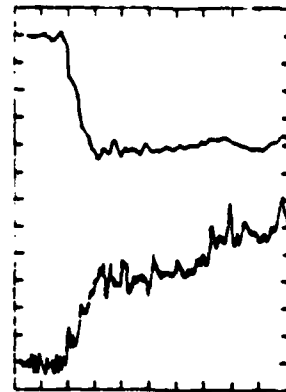

Fig. 5. Cathode turn-on data for carbon brush with 10 cm A-K gap. (100 ns/div)
Upper trace: Voltage (160 kV/div)
Lower trace: current (2.28 kA/div)

The initial detectable current always coincided with the knee (at about 30 ns) during the rise of generator voltage. Rapid current fluctuations were measured for both types of cathodes. The spiky nature of the current agrees with the NRL induction linac results in which a similar brush cathode was compared with a thermionic cathode [11]. The cause of the current fluctuations could be nonsimultaneity in the explosive emission from the multiple tufts of carbon string. Voltage compensation at early times is seen to be excellent, with flat voltage ($\pm$ 5 %) over a 0.7 μs pulse.

Electron beam uniformity was measured by means of the lucite plate diagnostic. Figure 6 gives an open shutter photograph of the lucite plate for a MELBA pulse which crowbarred at 0.5 μs.
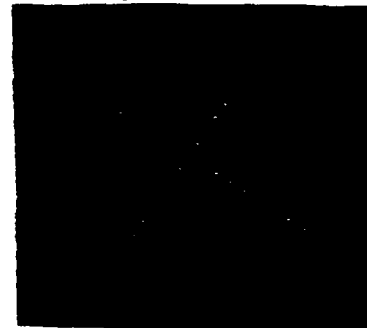

Fig. 6. Open shutter photograph of lucite plate for 0.5 μs electron beam pulse. Brush cathode with 10 cm A-K gap.

The lucite plate data indicates that the electron beam has good uniformity over the full cathode diameter. For longer electron beam pulses, the large electrostatic charge deposited in the lucite caused arcing between the apertured beamlets, obscuring the data and damaging the lucite.

Diagnostic data for two noncrowbarred electron beam pulses from MELBA are presented in Fig. 7.

Large current spikes are believed to be
cathode flares from individual tips and were
also observed in lower current density Soviet
experiments. The apertured e-beam signal
exhibited large fluctuations during enhanced
current. These large current fluctuations
could be caused by a streaming instability.
[20]

Diode Closure Velocities

For purposes of this research it is
useful to define two closure velocities:
1) The effective closure velocity v, is
defined by the shorting time of the A-K gap.
2) Apparent closure velocity u, is that which
is defined in terms of the Child-Langmuir
current with a closing A-K gap, is
obtained from the slope of $(P)^{-1/2}$, where
P is the perveance.

The data of the Type A shot in Fig. 7
shows that the voltage, hard X-rays, and
apertured e-beam current persist for 3.7
μs with a 10 cm A-K gap; this yields an
effective closure velocity of 2.7 cm/μs.

Figure 8 gives the time history of the
diode impedance and $(P)^{-1/2}$, for the same
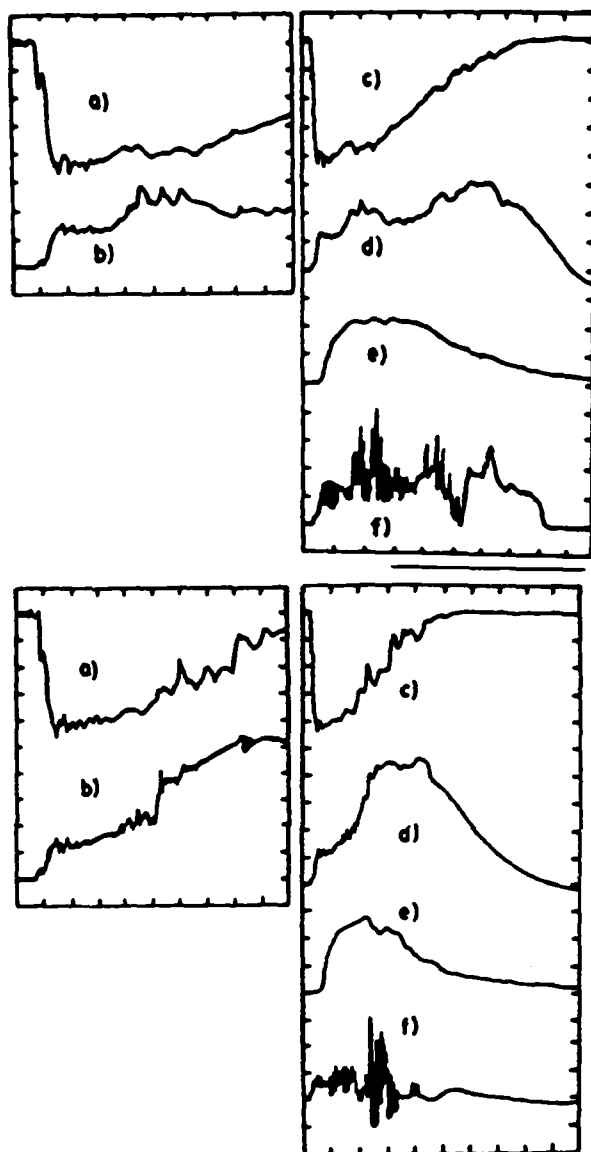two shots given in Fig. 7.

Fig. 7 MELBA electron beam pulse without
crowbar, upper data represent Type A
shot; lower data set represents Type
B shot.
a) Voltage (160 kV/div; 0.2 μs/div)
b) Current
   (5.3 kA/div; 0.2 μs/div)
c) Voltage (160 kV/div;0.5 μs/div)
d) Current (6.2 kA/div; 0.5 μs/div)
e) Hard X-rays (0.5 μs/div)
f) Apertured e-beam current
   (20 A/div,0.5 μs/div), no foil.
Parameters: Brush cathode on 7 cm
radius plate, A-K gap of 10 cm.
Charging voltages:
$V_m = \pm 56$ kV and $V = \pm 56$ kV
Two types of current behavior were ob-
served: Type A with flat or decreasing
current late in the pulse, and Type B with
current continually increasing throughout the
pulse. For brush and velvet cathodes, the
voltage flatness was limited by large cur-
rent spikes and the rapid increase which
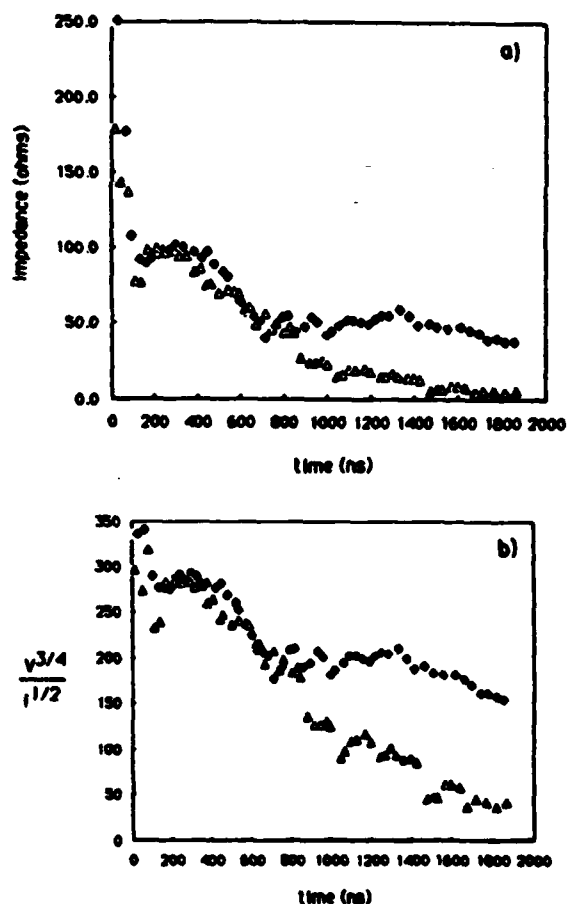typically occurred.

Figure 8. Temporal evolution of data from
Fig. 7: a) Impedance profile for
type A shot (solid points) and type
B shots (open points), b) $P^{-1/2}$

Note that type A shots gave a flat impedance
(50 ohms) after about 0.8 μs whereas type B
shots gave continually drooping impedance.
In type A shots the slope of $P^{1/2}$ appears to
change at about 0.8 μs. This has been
interpreted by others as an actual slowing of
the cathode plasma velocity by "electric
pressure" [21] or by the beam magnetic field
[22]. For a 10 kA beam current the magnetic
pressure is much less than the kinetic
pressure of typical cathode plasma.
However, the relativistic Child-Langmuir
analysis of the next section shows that the
type A current can be modeled by a constant
closure velocity at early and late times.

Table 1 summarizes the apparent and
effective diode closure velocities for brush
and velvet cathodes at different A-K gap
spacings.

Table 1

Summary of Diode Closure Velocities (cm/μs)

A-K gap (cm)	BRUSH		VELVET	
	10	8	10	8
Apparent				
Type A	3.3 ±.4 (3)	3.3 (1)	None	
Type B	5.3 ±.4 (2)	6 (1)	6.1 (1)	6.2 (1)
Effective				
Type A	3 ± .7 (3)	2.1 ±.3 (7)	None	
Type B	3.5 ±.6 (4)	2.6 (1)	3 ±.6 (4)	4.1±.3 (5)

(Numbers in parentheses indicate shots
averaged)

It should be noted that the velvet
cathodes always gave continually increasing
current (type B) behavior. In spite of the
higher electric field a number of brush
cathode shots with d_{ak} = 8 cm demonstrated
lower closure velocities than the same
cathode with d_{ak} = 10 cm.

Diode Current Data and Modeling

Our model for current flow from a
moving source plasma in the diode employs
a fully relativistic version of the Child-
Langmuir current density which can be
modified by the inclusion of ion flow [23].
Following the technique of Poukey, we perform
a Romberg integration solution for the
current density corresponding to space charge
potentials in a planar diode gap. For our
model we have also included closure of the A-
K gap by the cathode plasma with velocity u
and ion flow of variable magnitude [23-25].
Edge emission was modeled by the technique of
Parker [26].

Two types of temporal current behavior
were observed in these experiments. Figure 9
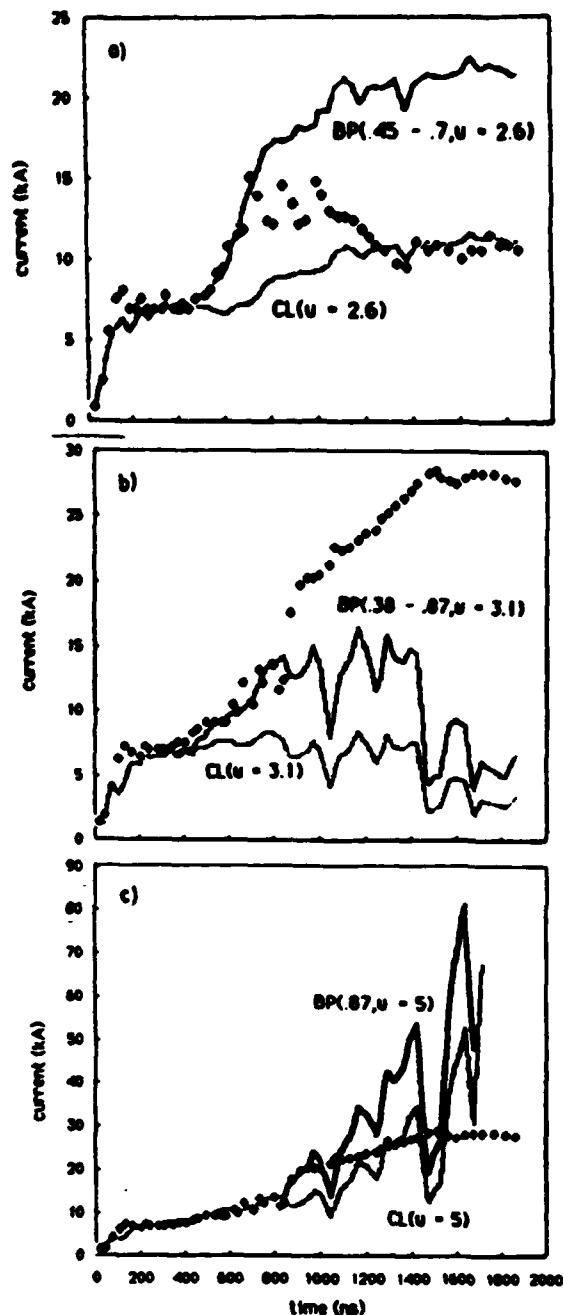compares type A and type B current traces
with theoretical models.

Fig.9 a) Experimental current data (points)
from type A shot compared with constant
closure velocity model (u = 2.6 cm/μs)
for Child-Langmuir (CL) current and
bipolar flow (BP) turned on linearly
from 0.45 μs to 0.7 μs.

b) Experimental current data from type
B shot compared to Child-Langmuir (CL)
with closure velocity of 3.1 cm/μs and
bipolar (BP) flow turned on linearly
from 0.38 μs to 0.87 μs with constant
closure velocity.

c) Experimental current data from type
B shot compared to Child-Langmuir (CL)
with a constant closure velocity of 5
cm/μs and bipolar flow (BP) turned on at
0.87μs.

Note from Fig. 9a that the experimental current agrees with the Child-Langmuir model from 0 to 0.45 μsec and from 1.2 μs to 1.9 μs. However, between 0.45 μs and 0.7 μs, a linear transition to bipolar flow models the data very well. A physical explanation for the type A current behavior is that at early times (less than 0.45 μs) the cathode emits the Child-Langmuir current. Between 0.6 μs and 0.7 μs ions from the anode or the background gas $(3 - 8 \times 10^{-5}$ Torr) are sufficient to support bipolar flow. At later times (greater than 0.7 μs) "ion starvation" causes the current to return to Child-Langmuir flow.

In type B shots the early time behavior is similar to type A. The type B shots, however, exhibit continually increasing current throughout the pulse. Figure 9b shows that even a transition to bipolar flow (at constant closure velocity) cannot model this rapid current increase. An increased closure velocity of 5 cm/μs, modeled in Fig. 9c, would provide a physical mechanism for the rapid current increase. This agrees with Ref. 27 in which the authors conclude that for cases in which a threshold energy dose rate is exceeded, the anode plasma gives both a transition to bipolar flow and an increased diode closure velocity. It should be noted that the energy density to the anode in our experiments is well below the required 400-600J/gm dose for graphite [27]. The longer pulselengths in our experiments may reduce the threshold energy for anode plasma production. For microsecond pulselengths it is also possible that background gases play a role ion production.

The interpretation of enhanced current in terms of anode plasmas is supported by the observation that the apertured e-beam signal always showed enhanced fluctuation levels during the period of increasing current. These large fluctuations could be indicative of a streaming interaction between the beam and the anode plasma [20]. Etching of the CR-39 track film embedded in a cathode gave a crater over the entire exposed area suggesting a large flux of low energy ions backstreaming to the cathode.

Some additional observations concern the conditions under which type A and type B currents were measured. Velvet cathodes always gave type B current. For 8 cm A-K gaps the brush cathode was more likely to give type A behavior (7 out of 8 shots).

Brush cathode experiments with 10 cm A-K gaps showed that on the first several shots after opening the diode to air, a type A shot was more likely; on later shots a type B shot was more likely. Apparently the cathode current density, surface chemistry and residual gas play a role in microsecond plasma production.

Transient Circuit Codes and Voltage Compensation

The generator system performance was calculated with the SPICE transient circuit analysis program. The computational model includes stray capacitances, inherent inductance loops, effective Marx shunt impedance, and the RC filter circuit. The values of the various elements were derived by PSI [17] from a combination of measurements, experimental data, extrapolations, and calculations. The SPICE circuit code has been run for fixed resistance loads as well as time varying impedances. For the time-varying diode impedance, the load is modeled in a piecewise linear manner using a nonlinear circuit element (typically a JFET).

Current spikes and irreproducibility in the diode current made direct experimental comparison of different compensating voltages difficult on separate shots.

Figure 10 compares the experimental voltage with transient circuit analysis code results using the experimental impedance profile for two cases:

1) Actual MELBA circuit and charging voltages, and
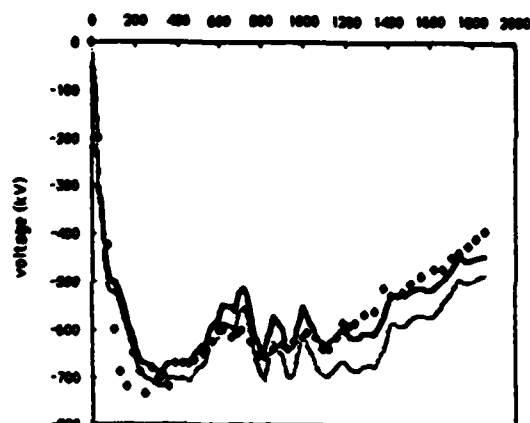2) MELBA circuit but increased charging voltage of ringing stage.

Fig. 10. MELBA experimental voltage (points) for type A shot compared to SPICE code using experimental impedance profile with: Actual charging voltages (dark line) $V_M = \pm 56$ kV, $V_R = \pm 56$ kV, and, increased charging voltage on the reversed stage, $V_M = \pm 56$ kV, $V_R = +90$ kV It can be seen that increasing the ringing reverse stage charging voltage improves the voltage flatness between 0.8 μs and 1.4 μs. However, the voltage deviations observed in these experiments have been caused primarily by current spikes and the rapid current enhancement starting at 0.45 μs. Current spikes may be eliminated by resistively ballasting the individual emitters on a multitip or brush cathode.

References

1) H. Friedman and M. Ury, "Microsecond duration intense relativistic electron beams," The Review of Scientific Instruments, Vol. 43, No. 11, pp. 1659-1661, August 9, 1972.

2) T. H. Martin and R. S. Clark, "Pulsed microsecond high-energy electron beam accelerator," The Review of Scientific Instruments, Vol. 47, No. 4, pp. 460-463, April 1976.

3) R. Schneider, C. Stallings, and D. Cummings, "Generation and extraction of microsecond intense relativistic electron beams," Journal of Vacuum Science Technology, Vol. 12, No. 6, pp. 1191-1193,, Nov./Dec. 1975.

4) Juan J. Ramirez and Donald L. Cook, "A study of low-current-density microsecond electron beam diodes," Journal of Applied Physics, Vol. 51, No. 9, pp. 4602-4611, September 1980.

5) M. A. Vasilevskii, I. M. Roife, and V. I. Engel'ko, "Operating characteristics of explosive-emission multipoint cathodes with microsecond pulse lengths," Zh. Tekh. Fiz. 51, 1183-1194 (Soviet Journal of Technical Physics, Vol. 26, No. 6, pp. 671-678), June 1981.

6) V. S. Noronin, S. M. Zakharov, L. N. Kazanskii, and S. A. Pikuz, "Intense monoenergetic microsecond electron beam with stabilized current," Pis'ma zh. Tekh. Fiz. 7, 1224-1227 (Soviet Technical and Physical Letters, Vol. 7, No. 10, pp. 523-524), October 1981.

7) S. V. Lebedev, V. V. Chikunov, and M. A. Shcheglov, "Microsecond-length relativistic electron beams from a plane diode," Pis'ma Zh. Tekh. Fiz. 8, 693-696 (Soviet Technical and Physical Letters, Vol. 8, No. 6, pp. 302-303), June 1982.

8) V. A. Burtsev, M. A. Vasilevskii, O. A. Gusev, I. M. Roife, E. V. Seredenko, and V. I. Engel'ko, "High-current relativistic electron beam with length greater than 10^{-5} sec," Pis'ma Zh. Tekh. Fiz. 2, 1123-1126 (Sov. Tech. Phys. Lett., Vol. 2, No. 12, pp. 441-442), December 1976

9) E. A. Abramyan, E. N. Efimov, and G. D. Knieshav, "Energy recovery and power stabilization of pulsed electron beams in Marx generator circuits," in Proceedings of the 2nd International Topical Conference on High Power Electron and Ion Beam Research and Technology, Vol. 2, Oct. 3-5, 1977, pp. 755-760.

10) Ian Smith, "Pulse power for 0.3-0.5 us. durations," Lawrence Livermore Laboratory Report, UCID - 18318, October 1979

11) C. W. Roberson, J. A. Pasour, F. Mako, R. F. Lucey, Jr., and P. Strangle, "A free-electron laser driven by a long-pulse induction linac," Infrared and millimeter waves, Vol. 10, Academic Press, Inc., 1983, Ch. 7, pp. 361-397.

12) R. Prohaska and A. Fisher, "Field emission-cathodes using commercial carbon fibers," Rev. Sci. Instrum., Vol 53, No. 7, pp. 1092-1093, July 1982.

13) E. N. Abdullin, G. P. Bazhenov, S. P. Bugaev, and O. B. Ladyzhenskii, "Formation of millisecond electron beams through explosive electron emission," Pis'ma Zh. Tekh. Fiz. 7, 347-350 (Sov. Tech. Phys. Lett., Vol. 7, No. 3, pp.

148-149), March 1981.

14) Yu. A. Vasilevskaya, M. A. Vasilevskii, I. M. Roife, V. I. Engel'ko, S. P. Yakovlev, and E. G. Yankin, "Electron beam formation in a diode with a multiple-tipped explosive emission cathode," Zh. Tekh. Fiz. 53, 677-682 (Sov. Phys. Tech. Phys. Vol. 28, No. 4, pp. 429-432), April 1983.

15) G. P. Bazhenov, S. P. Bugaev, G. A. Mesyats, and S. M. Chesnokov, "Use of explosive emission to produce current pulses longer than 10^{-4} sec," Pis'ma Zh. Teckh. Fiz. 2, 462-465 (Sov. Tech. Phys. Lett., Vol. 2, No. 5, pp. 180-181), May 1976

16) V. A. Burfsev, M.A. Burfsev, M. A. Vasilevskii, I. M. Roife, E. V. Seredenko, and V. I. Engel'ko, "Improved stability of explosive-emission multiple-tip cathodes," Pis'ma Zh. Tekh. Fiz. 4, 1083-1087 (Sov. Tech. Phys. Lett. Vol. 4, No. 9, pp. 436-37), September 1978.

17) Phillip Champney, "Electron beam accelerator," Pulse Sciences Inc. Proposal: PSI-P-83-105, August 1983.

18) E. Cohen, A. Vladimirescv, D. O. Pederson, "User's guide for SPICE circuit simulation program," Univ. of Calif., Berkeley.

19) V. A. Nemchinskii, "Anode spot in a high-current vacuum arc," Zh. Tekh. Fiz 52, 35-42 (Sov. Phys. Tech. Phys. Vol. 27, No. 1, pp. 20-25), January 1982.

20) R. J. Briggs, "Electron Stream Inter-action with Plasmas," Research Monograph No. 29, MIT Press, Cambridge, MA., 1964.

21) D. D. Hinshelwood, "Explosive Emission Cathode Plasmas in Intense Relativistic Electron Beam Diodes," Ph.D. Thesis, MIT, 1984.

22) D. Mosher, (Private Communication)

23) J. W. Poukey, "Ion effects in relativistic diodes," Applied Physics Letters, Vol. 26, No. 4, 11, 15, pp. 145-146), February 1975.

24) D. S. Prono, H. Ishizuka, E. P. Lee, B. W. Stallard, and W. C. Turner, "Charge-exchange neutral-atom filling of ion diodes: its effect on diode performance and A-K shorting," J. Appl. Phys., Vol. 52, No. 4, pp. 3004-3011, April 1981.

25) Irving Langmuir, "The interaction of electron and positive ion space charges in cathode sheaths," Physical Review, Vol 33, pp. 954-989, June 1929.

26) R. K. Parker, R. E. Anderson, and C. V. Duncan, "Plasma-induced field emission and the characteristics of high current relativistic electron flow," J. Appl. Phy. 45, 2463 (1974).

27) D. Dakin and J. Benford, PI Memo, Oct. 1976

Beam Erosion Due to Scattering
in Low Pressure Media

M. Cuneo, J. Les, and T. Kammash
The University of Michigan
Ann Arbor, Michigan 48109

Abstract

A Monte Carlo Fokker Planck code is used to investigate the scattering loss of particles from a relativistic electron beam propagating in a low pressure air channel. The fraction of particles transmitted is calculated and its variation with relevant beam and channel parameters is obtained. The effect of multiple scattering is examined, and a parameter reflecting scattering erosion rate is calculated for some experimentally observed parameters and found to agree with an analytical expression for force-free propagation.

Introduction and Analysis

Some of the most comprehensive results on beam erosion in the Ion-Focused Regime (IFR) have recently emerged from the ETA experiment at Livermore.[1] In air this regime for stable propagation corresponds to a pressure window of about 0.1-0.2 torr. At 0.08 torr beam erosion primarily at the head of the beam was observed and found to correspond to 0.16 m/m. At these low pressures it is expected that most of the erosion will be due to ohmic heating; however it is also important that some assessment of the role of scattering in erosion be made particularly as the parameters of the beam or the channel vary. In this paper we examine the loss of particles from the beam as it transverses a preformed channel and attempt to deduce quantities which may have a direct bearing on erosion. The investigation is carried out with the aid of a Monte Carlo Fokker Planck code which allows us to follow a given sample of non-interacting beam particles in full configuration and velocity space as the beam propagates in a cylindrically symmetric gaseous channel. It is assumed that the channel medium is partially ionized so that interaction of the beam particles with charged and neutral target particles are taken into account. The probability of neutral particle interaction is selected by defining an appropriate mean free time

$$t_f = \frac{1}{v \sigma n} \qquad (1)$$

where U is the beam electron velocity, n is the neutral density and σ is an appropriate interaction cross section. Although other inelastic events should generally be considered we limit our study to ionization and the interaction probability is given by dt/t_c when dt is a very small code time step. Given an appropriate differential scattering cross section a random scattering angle θ can be selected from the distribution

$$p(\theta) = \frac{\int_{\theta_{mi}}^{\theta} \frac{d\sigma}{d\Omega} d\Omega}{\int_{\theta_{mi}}^{\theta_{max}} \frac{d\sigma}{d\Omega} d\Omega = \sigma_{tot}} = \xi \quad ; \quad \theta_{max} = \frac{274}{A^{1/3}} \frac{c}{\gamma U}$$

where ξ is a random number. For relativistic electrons propagating in a low temperature medium it is expected that the distribution be highly peaked in the forward direction and using the results from hydrogen appropriately scaled for higher z elements we can write[2]

$$\int_{\theta_{mi}}^{\theta} \frac{d\sigma}{d\Omega} d\Omega = \int_{\theta_{mi}}^{} \frac{128 \pi^5 m^2 z^5 e^4}{h^4 k^4} \frac{\cos\theta}{\sin^3\theta} \left[1 + \frac{1}{(1 + \frac{1}{4} k^2 a^2 \sin^2\theta)^4} \right] d\theta$$

$$= \frac{\delta\beta}{2} \left\{ -\frac{1}{1 + \beta\theta_{mi}^2} + \frac{1}{1 + \beta\sin^2\theta} + 4 \log\left[\frac{(1 + \beta\theta_{mi}^2)\sin^2\theta}{(1 + \beta\sin^2\theta)\theta_{mi}} \right] \right.$$

$$\left. + \frac{1}{3} \left[-\frac{1}{(1 + \beta\theta_{mi}^2)^3} + \frac{1}{(1 + \beta\sin^2\theta)^3} \right] \right\} \qquad (2)$$

where in CGS units

$$\delta = \frac{3.2885 \times 10^{20}}{U^4} \quad ; \quad \beta = (1.74 \times 10^{-16})\, U^2$$

In the above expression m is the electron mass, k is the DeBroghi wave number, h is Plancks constant, $a \simeq 1.4\, a_0 z^{1/3}$, a_0 is the Bohr radius and θ_{mi} is the minimum scattering angle given by

$$\theta_{min} \simeq \frac{Z^{1/2}}{192} \frac{c}{v\gamma}$$

where γ is the relativistic parameter and c is the speed of light. Although small angle Coulomb scattering is included in the code by an implicit Fokker Planck method the probability for such scattering event in the code time step dt is simply dt/τ_d where τ_d is the well known deflection time. For plasma densities on the order of $10^{11}-10^{15}$ cm^{-3} which are appropriate for the case at hand, and for $v \simeq c$ it is easily seen that $\tau_d \simeq 10^{-1}$ seconds so that at pulse lengths on the order of nanoseconds it is clear that scattering from charged particles can be neglected. These considerations are consistent with some experimental observations.[3]

In order to crudely model the propagation of a relativistic electron beam in either an IFR or a force-free propagation mode we have incorporated the self magnetic field in a phenomenological way using Ampere's law for an infinite, uniform beam. We have neglected the radial electric field by taking a charge neutralizing ion density (n_i) to be equal to the beam density (n_b) so that the charge neutralization parameter $f \simeq 1$. Since the code calculates the number of particles that traverse the channel the fraction of the beam that is transmitted would then represent an upper limit for pulse lengths τ_p that are shorter than τ_{CN}, the charge neutralization time, and a good estimate when $\tau_p \simeq \tau_{CN}$ since the physics of instabilities that might occur are not included. Under these conditions the description of the scattering process might be deemed appropriate to that taking place in a force neutralized $f_e > 1/\gamma^2$, charge neutralized, $f_e \simeq 1$ or force free $f_e \simeq 1$, $f_m \simeq 1$ regimes. With propagation having been observed in pressure ranges of 0.1-5 torr[4,5] it should be noted that at lower pressures there are usually insufficient neutrals to provide an adequate ion density for force neutralization and at higher pressures multiple scattering could cause rapid dispersal of the beam. The latter effect is, however, incorporated in the code and its influence will be discussed later.

In assessing the utility of the Monte Carlo-Fokker Planck code in the beam propagation study it should be kept in mind that particle scattering can be accurately described and that no assumptions need be made concerning the plasma conductivity since ionization can be calculated self-consistently. Particle and energy loss mechanisms can also be readily included so long as the appropriate mean free paths for these processes can be selected. Because of its three dimensional simulation capability the often-used "paraxial" approximations and others need not be made. Because of its limitation in the number of particles that can be simulated it is clear that the

3

treatment of self fields and the modelling of instabilities, though possible, might be quite difficult.

Some Preliminary Results

A relevant factor to beam erosion by scattering is whether the beam particle undergoes single or multiple scattering events as it transverses the channel. If we denote by "T" the transmitted fraction of the beam, n_m the number of times scattering off of a neutral particle occurs, n_s the number of electrons used to simulate the beam, r_c the radius of the channel and $s = n_m/n_s$ then the variation of these parameters with r_c for a beam radius $r_b = 1.5$ cm, total cross section $\sigma_{tot} = 3 \times 10^{-18}$ cm^2, neutral density $n_n = 2 \times 10^{15}$ cm^{-3} and $n_s = 5000$ is shown in Table 1.

Table 1

r_c	T	n_m	s
2.5	0.007	7338	1.47
5	0.015	9258	1.85
10	0.03	12183	2.4
15	0.079	15003	3.0
21.2	0.14	17800	3.56

We observe that the transmitted fraction is linearly proportional to r_c^2 which is a direct consequence of the geometric effect. Another geometric consequence is the linear scaling of n_m and s with r_c. Since the probability of neutral-interaction is proportional to the path length traversed, and the path length increases with r_c then the probability of multiple scattering should increase with r_c. The variation of these parameters with the neutral density is shown in Table 2 for a channel radius $r_c = 21.2$ cm and beam radius and total scattering cross section as before.

Table 2

n_n (cm^{-3})	n_m	s	T
2×10^{13}	293	0.06	0.95
2×10^{14}	2789	0.66	0.79
2×10^{15}	18000	3.6	0.14
2×10^{16}	68263	13.65	0.002

The transition from single to multiple scattering, $s = 1$, is clearly noted in the table. Although the distribution for single scattering is highly peaked in the forward direction, beam particles may still gain sufficiently large transverse directed energy to cause substantial beam breakup.

The code was also utilized to estimate an "erosion rate" due to scattering. It yields the fraction of the beam lost per unit length travelled. When this fraction is multiplied by the length of the beam a loss rate due to scattering is obtained. This is given by

$$\alpha = \beta L_p = \frac{\Delta T}{2 \Delta z} L_p \qquad (4)$$

where "β" is the fraction of particles lost per meter, and $v \tau_p = L_p$ is the length of the pulse in meters. Equation (4) is based on the assumption that for constant beam density and constant loss rate of particles the loss rate of particles in a rigid beam is equivalent to the loss rate of beam length. When the parameters of the force free propagation experiment of Ref. 4 are used, Eq. (4) yields results comparable to those predicted by the analytical expression given by Lee[6] that is based on the SNEEZE code.

References

1. K. W. Struve, E. J. Lauer, and F. W. Chambers UCRL-88922, Sept. 1983.
2. N. F. Mott and H. S. W. Massey, The Theory of Atomic Collisions, 3rd edition, Oxford Press, 1965.
3. P. A. Miller, and J. B. Gerardo, J. Appl. Physics, 43, 3008 (1972).
4. W. Link et al, IEEE Trans. NS 14, 777 (1967).
5. T. Fessenden et al, UCID-17840, June 1978.
6. E. P. Lee, UCID-18768, August 1980.

Pittsburgh Hilton

June 3-5, 1985

Gas Hydrodynamics of Channels Formed by
Rapid Heating by Lasers and Laser Guided
Discharges,* L.D. HORTON and R.M.
GILGENBACH, Department of Nuclear
Engineering, The University of Michigan,
Ann Arbor, MI, 48109.

The hydrodynamic evolution of
reduced density channels produced by CO_2
laser induced gas breakdown and by laser
guided discharges have been studied. In
the laser induced breakdown experiments,
a high power (0.30 GW) TEA CO_2 laser is
brought to a quasi-line focus over 14 cm
in argon by a compound reflecting axicon
with a W-shaped cross section (waxicon).
Electrical discharges of 30 kV are
initiated and guided by CO_2 laser
induced air breakdown focused by a
conventional mirror with 2.5 m focal
length.

Experimental data are obtained
using schlieren photography and
collinear holographic interferometry.
Shock positions and directly measured
(non-Abel inverted) channel density
profile data are compared to a one
dimensional hydrodynamics code in order
to estimate fractions of available
energy absorbed into channel heating.
This one dimensional code is valid for
times short compared to the onset time
for convective mixing which eventually
cools and breaks up the reduced density
channel.

For waxicon focused laser induced
gas breakdown channels the measured
shock wave velocity ranges from 0.4 to
0.5 mm/μs. Comparison to the
computational model indicates that 25-
30% of the laser energy is absorbed into
heating the channel.

For laser guided discharges the
measured density at the center of the
channel is 0.025 kg/m^3. This is in
excellent agreement with the one
dimensional code for times small
compared to the time scale for
convective mixing. However, at later
times the code predicts narrower
channels with lower on-axis densities
than are measured.

*This research is supported by the
Office of Naval Research, National
Science Foundation Grant ECS-8309682,
and a Presidential Young Investigator
Award funded by General Motors Research
Labs and the National Science
Foundation.

Subject category and number:

1. Magnetohydrodynamics

☐ Prefer oral session

☑ Prefer poster session

☐ No preference

Submitted by:

Ronald M. Gilgenbach

University of Michigan

Dep't of Nuclear Eng.

Ann Arbor, MI 48109

(313) 763-1261

Important:

The Conference Record will be produced by direct
photoreduction of submitted abstracts, so the quality of the
final text is the responsibility of each individual author. The
abstract must fit within the box on the left and should be
typed in a face that is no smaller than 12 pitch (12
characters per inch). A format sample is given in the Call for
Papers announcement.

Spatially and Temporally Resolved Diagnostics
for Microsecond, Intense Electron Beams *

R. M. GILGENBACH, M. BRAKE, L. D. HORTON,
S. BIDWELL, R. F. LUCEY, L. SMUTEK, and
J. E. TUCKER, Nuclear Engineering Department,
University of Michigan, Ann Arbor, MI 48109

Experiments are underway to investigate new
diagnostics for electron beams in vacuum and
in a plasma background. Measured parameters
include temporally resolved beam current
profile and beam emittance. These character-
izations are being performed during electron
beam diode closure experiments (1) and beam-
plasma interaction experiments with either of
two long-pulse accelerators: MELBA (Michigan
Electron Long Beam Accelerator):
Voltage = - 1 MV, Current = 10 kA, at
Pulselength = 0.1 to $1 \mu s$ $(1.4 \mu s)$ for
voltage flat to within ± 7% (± 10%) .
The second accelerator is a long-pulse
Febetron with parameters: Voltage = - 0.5 MV,
Current= 1 kA, and Pulselength = 0.3   s.
     Two different configurations have been
developed which use Cerenkov radiation to
detect electron beam current profiles as a
function of time. The first uses Cerenkov
emission by electrons which impinge axially
on a single fiberoptic lightguide enclosed
in a lucite tube. Plasma light is blocked
by graphite spray or thin foil covering the
end of the optical fiber. This diagnostic
has the the following advantages:
1) the threshold energy for Cerenkov emission
effectively discriminates between high energy
beam electrons and low energy (3-5 eV)
plasma electrons. 2) The small, nonconducting
probe introduces a minimal perturbation into
the beam-plasma system, 3) Excellent signal
to noise ratio is obtained because the
fiberoptic signal is directly transmitted
to a photomultiplier tube in the Faraday cage.
4) Quantitative data is obtained directly.
     The second Cerenkov diagnostic employs
an array of small apertures in the anode
plate. The apertured beamlet array strikes a
clear Cerenkov plate located several cm behind
the anode. This plate is covered by a thin
layer of graphite to pass electrons but not
diode light. The back of the Cerenkov plate
can be viewed by open shutter or streak
photography. This diagnostic thus has the
potential for temporally resolved measurements
of both beam current density and emittance.
     Time resolved optical emission spectro-
copy is used to determine plasma composition,
degree of ionization, and equilibrium con-
ditions of long pulse REB produced plasmas
at pressures above 0.1 Torr. A gated inten-
sified diode array detector is employed with
a 275mm, f/3.8 spectrograph.

(1) R. M. Gilgenbach et al., Invited paper:
 "Microsecond Electron Beam Diode Closure
  Experiments", IEEE Pulsed Power Conference,
  June 10-12, 1985, Arlington, VA

Pittsburgh Hilton

June 3-5, 1985

Subject category and number:

6. Electron, Ion, Sources

or 8. Intense Electron Be

☐ Prefer oral session

☑ Prefer poster session

☐ No preference

Submitted by:

RONALD M. GILGENBACH
NUCLEAR ENGINEERING DEPT.
UNIVERSITY OF MICHIGAN
ANN ARBOR, MI 48109

(313) 763-1261

RONALD M. GILGENBACH
NUCLEAR ENGINEERING DEPT.
UNIVERSITY OF MICHIGAN
ANN ARBOR, MI 48109

Important:

The Conference Record will be produced by direct
photoreduction of submitted abstracts, so the quality of the
final text is the responsibility of each individual author. The
abstract must fit within the box on the left and should be
typed in a face that is no smaller than 12 pitch (12
characters per inch) A format sample is given in the Call for
Papers announcement.

"MICROSECOND ELECTRON BEAM INTERACTIONS WITH MONATOMIC
AND DIATOMIC GASES"

R. M. Gilgenbach, L. D. Horton, M. L. Brake

R. F. Lucey, and J. E. Tucker

MICROSECOND ELECTRON BEAM INTERACTIONS WITH MONATOMIC AND DIATOMIC GASES *

R. M. GILGENBACH, L. D. HORTON,
M. L. BRAKE, R. F. LUCEY, AND
J. E. TUCKER, UNIVERSITY OF
MICHIGAN, ANN ARBOR, MI 48109

Microsecond electron beam experiments are
being conducted on MELBA (Michigan Electron
Long Beam Accelerator). This new Long Pulse
accelerator operates with parameters:
Pulselength = 0.1 to 1.4 microseconds
Voltage = −1 MV flat to < + 10 % at
Current = 10 kA.
Unique circuitry permits electrical
compensation for diode impedance droop.
Initial interaction experiments used Febetron
beams with 0.3 microsecond pulsewidths at
voltages < 500 kV and currents < 1.4 kA.
Interaction data with argon and nitrogen at
0.5 Torr to 40 Torr show induced plasma
currents which persist for > .1 microsecond
after the beam pulse ends. Argon gives longer
decay times than nitrogen. New industrial
processing applications of long−pulse beams
are being explored.

Hydrodynamics of Rapid Energy
Deposition in Gas Channels

L. D. Horton and R. M. Gilgenbach

Technical Report

Intense Energy Beam
Interaction Laboratory
Nuclear Engineering Department
University of Michigan
Ann Arbor, MI   48109

Hydrodynamics of Rapid Energy Deposition in Gas Channels

L.D. Horton and R.M. Gilgenbach
The University of Michigan
Department of Nuclear Engineering
Ann Arbor, Michigan 48109

ABSTRACT

Reduced density channels produced by laser induced gas breakdown and by laser guided discharges are modelled by means of a one dimensional gas hydrodynamics code for times earlier than the onset of convective mixing. Comparison of laser induced gas breakdown experiments with the code indicate that the conversion of laser energy to gas heating is limited to 25-30%. Collinear holographic measurements of channel density profiles produced by laser guided discharges are found to be in good agreement with code predictions for times less than 50 μs. This agrees with other experiments which have indicated onset times for convective mixing in the range 50-70 μs after the start of the discharge.

Introduction

Extensive experiments at the Naval Research Labs (NRL) have studied channels formed by the rapid deposition of energy in atmospheric pressure gas.[1-6] Laser guided discharges and the resulting reduced density channels have applications in electron and light ion beam transport[3,7-9], in lightning modelling[10], and in materials processing[11,12]. Here we report results for the nonturbulent phase of reduced density channels formed by laser induced gas breakdown[13] and by laser guided electrical discharges[14]. Data is analysed and interpreted using a one dimensional, cylindrically symmetric gas hydrodynamics code. This code uses the standard conservation equations in Lagrangian coordinates with the addition of an artificial viscosity[15] to treat shock waves.

Computations by Picone et al[4,16,17] at NRL have shown that vorticity leads to turbulent convective mixing[10] which is the dominant decay mechanism for reduced density channels. Since our one dimensional hydrodynamic model cannot include vorticity, we model only the pre-mixing phase as determined from schlieren and holographic data. Collinear holographic interferometry is used in our experiments to directly measure the density profiles existing within the channel for comparison with the code.

I Experimental Configurations

Two different techniques are employed for rapidly depositing energy in a gas channel:

  1) CO_2 laser induced gas breakdown (Fig. 1a)

  2) laser guided discharges (Fig. 1b)

2

The CO_2 laser gas breakdown experiment uses a waxicon to produce a quasi-line focus[13] as depicted in Fig. 1a. A waxicon is a focusing mirror with a W shaped cross section. Argon is used as the gas for the waxicon experiments reported here. The schlieren diagnostic system employs a pinhole aperture to obtain two dimensional spatial resolution.

The laser guided discharge experiments employ a configuration (Fig. 1b) which permits the interferometric data to be taken in an orientation collinear to the discharge. A high power (0.30 GW) TEA CO_2 laser is focused by a 2.5 m focal length gold mirror. High voltage electrodes are located across the length of the resulting breakdown beads. A 0.04 μF capacitor charged to 30 kV is discharged across the electrode gap 5 μs after the CO_2 laser pulse. Discharge current is a damped sinusoid with peak current of about 10 kA, period of 1.4 μs, and 1/e decay time of 3.5 μs. The uniformity and decay time of channels generated by this experiment have been demonstrated[18] to closely resemble the longer channels at NRL[3]. Two pulse holographic interferometry is used to record the data. Between pulses the precision mirror is rotated slightly to produce secondary interference fringes on the film. Deflection of these fringes by the object gives a measure of the gas density. Due to the length of the object when the channel is viewed in this orientation and the resulting large fringe deflections, helium, which has a low index of refraction, is used as the ambient gas. Note that Abel inversion of holographic data is not required in the collinear arrangement since the data directly yields the

3

density profile in the interior of the channel.

II Numerical Model

The gas hydrodynamics code uses the standard conservation of mass, momentum, and energy equations in Lagrangian coordinates and cylindrical symmetry.

$$\frac{d\rho}{dt} = -\frac{\rho}{r}\frac{\partial(ru)}{\partial r}$$

$$\frac{du}{dt} = -\frac{1}{\rho}\frac{\partial(p+q)}{\partial r}$$

$$\frac{dp}{dt} = -(\gamma p + (\gamma-1)q)\frac{1}{r}\frac{\partial(ru)}{\partial r}$$

$$\frac{dr}{dt} = u$$

Here p is the gas pressure, ρ is the gas density, u is the local velocity, and γ is the ratio of specific heats. Note that q is an artificial viscosity, originally proposed by VonNeumann and Richtmyer[15], which is taken to be quadratic in the time derivative of the density so that discontinuites at shock fronts are smoothed over a few mesh spacings. Using the continuity equation the artificial viscosity takes the form

$$q = c\,\rho\,(\Delta r)^2\left(\frac{1}{r}\frac{\partial(ru)}{\partial r}\right)^2$$

Here c is a constant varied as a parameter to ensure smooth behavior around the shock. For the results given in this paper c varies in the range 2 to 5. An explanation of the logic leading to this form of q is given in Ref. 19. However, q is, in fact, artificial and other variations have been employed.

The difficulty in modelling these experiments lies in the driving term. Standard blast wave theory assumes a source which is a delta function in time and simply sets initial conditions corresponding to an appropriate overpressure. This approach is

4

acceptable for our laser induced gas breakdown experiments but
the laser guided discharge experiment has an energy deposition
time which is comparable to hydrodynamic time scales. The time
dependence of the energy deposition for the laser guided
discharge is found by using the current histories and by assuming
that the channel resistance is constant so that $E=R\int_0^t I^2 dt$. The
actual current traces closely follow the form of a damped sine
wave which agrees with the assumption of a constant resistance.
Since the total absorbed energy is the parameter being varied in
the code, the absolute value of the channel resistance is not
required.

The spatial dependence of the energy deposition is not
straightforward. For the waxicon experiment the minimum
breakdown spot size is limited by machining irregularities in the
mirror and is estimated by schlieren photographs taken just at
the end of the CO_2 laser pulse to be 0.2 mm in diameter.
Doubling this spot size has only a small effect on the code
output and does not change the estimates of absorbed energy
fraction reported below.

The laser guided discharge energy deposition radius is a
function of time due to channel expansion during the discharge.
The channel radius is estimated using the data in Fig. 2 for an
air channel. Detailed transverse schlieren photographs for
atmospheric pressure helium are difficult to obtain at the ruby
laser probe wavelength (694.3 nm) but schlieren data does
indicate channels which are about 25% wider in helium than in
argon, N_2, or air. This factor is incorporated into the code's

5

estimate of radius of energy deposition. While it is
conceptually preferable to let the code calculate the channel
radius from the density data of the previous time step, Fig. 2
shows that the channel expands quickly to the laser breakdown
bead radius. The initial breakdown phase is not modelled in the
code for laser guided discharges and is clearly not one
dimensional. Therefore, an external input of early time channel
radii is necessary. Note that channel data from over a thousand
shots show reproducible straight, approximately one dimensional
channnels at times greater than about 10 s after the beginning
of the discharge (see the photographs in Fig. 2 for 31 and
51 μs). This indicates initial laser asymmetries are not
important in the nonconvective region of laser guided discharge
channel evolution[3-6,18].

III Results and Discussion

A comparison of experimental and code shock positions for
the waxicon breakdown experiment is shown in Fig. 3. The
available energy for the experimental points is calculated by
using laser calorimetry to normalize the power density on axis as
given by a ray tracing code[13]. As described in reference 13 the
waxicon mirror produces one region on axis where singly and
doubly reflected rays cross and another region with only doubly
reflected rays crossing the axis. Both of these regions
experience approximately constant energy depositions and
correspond to approximately straight shock fronts. Thus, two
data points are available for each incident laser energy. Shock
positions are very reproducible for a given laser energy setting.

6

The estimate of available energy is undoubtedly better for the longer region of only doubly reflected rays but both energy estimates have errors of less than 10%. Code results for various absorbed energies are superimposed on the experimental results in Fig. 3. Comparison between the data and the code indicates that only 25-30% of the available laser energy is going into heating the gas. Several potential energy loss mechanisms exist[20]. Ionization of the gas followed by recombination radiation which escapes the channel is one possibility but, for our short laser pulse length and small focal spot size this is expected to be negligible. Inaccuracies in the focusing mirror, producing off axis rays is another potential mechanism. The focal radius as predicted by early time schlieren photographs suggests that this also is a small contribution to the large energy fraction not heating the gas. The most likely mechanism for major energy loss is supercritical plasma reflection. Once the breakdown channel is completely singly ionized by the laser the resulting plasma is above critical density for 10.6 μm propagation and the remaining light is reflected rather than being absorbed. Only nonlinear processes can heat the channel once it has reached critical density which explains the poor coupling efficiency seen in Fig. 3.

The experimental data for the laser guided discharges are obtained using collinear holographic interferograms such as the one in Fig. 4. Relative densities are calculated by measuring fringe deflections from the reference at the edge of the channel. This reference density was originally estimated to be ambient but code results indicate a slight density reduction behind the shock

especially for times less than 50 μs. Thus the experimental data for Fig. 5 is normalized to the code prediction of the density just outside the channel. The code best reproduces the experimental results for an absorbed energy of 100 J/m. The available energy can be roughly estimated to be 110 J/m by noting that the final capacitor voltage after the discharge is 16 kV and by assuming about half of the discharged capacitor energy is dissipated in the spark gap switch. Agreement for channel density profiles is very good at 30 μs but for times later than 50 μs convective mixing has become important and the code predicts deeper, narrower reduced density channels than are actually measured. This onset time for convective mixing agrees quite well with data from transverse schlieren photographs which begin to show enhanced line integrated turbulence at about 70 μs after the start of the discharge[18].

Fig. 6 shows the pressure profile corresponding to the reduced density channel of Fig. 5(a). Note that by 30 μs the channel has already expanded to pressure equilibrium and has essentially finished its evolution in our convectionless, conductionless equations.

Acknowledgements

8

References

1) J.R. Greig, D.W. Koopman, R.F. Fernsler, R.E. Pechacek, I.M. Vitkovitsky, and A.W. Ali, Phys. Rev. Lett. $\underline{41}$, 174 (1978).

2) D.W. Koopman and K.A. Saum, J. Appl. Phys. $\underline{44}$, 5328 (1973).

3) M. Raleigh, J.R. Greig, R.E. Pechacek, and E. Laikin, NRL Memorandum Report No. 4380, February, 1981.

4) J.M. Picone and J.P. Boris, NRL Memorandum Report No. 4967, December, 1982.

5) M. Raleigh, NRL Memorandum Report No. 4781, April, 1982.

6) M. Raleigh, NRL Memorandum Report No. 4555, August, 1981.

7) G. Yonas, Sci. Amer. $\underline{239}$, 50 (1978).

8) P.A. Miller, R.I. Butler, M. Cowan, J.R. Freeman, J. W. Poukey, T.P. Wright, and G. Yonas, Phys. Rev. Lett. $\underline{39}$, 92 (1977).

9) J.N. Olsen and L. Baker, J. Appl. Phys. $\underline{52}$, 3286 (1982).

10) J.M. Picone, J.P. Boris, J.R. Greig, M. Raleigh, and R.F. Fernsler, J. Atmos. Sci. $\underline{38}$, 2956 (1981).

11) R.M. Gilgenbach, O.E. Ulrich, and L.D. Horton, Rev. Sci. Instrum. $\underline{54}$, 109 (1983).

12) M.L. Brake, R.M. Gilgenbach, L.D. Horton, and J.E. Tucker, Plasma Chem. and Plasma Proc. $\underline{3}$, 367 (1983).

13) R.M. Gilgenbach and L.D. Horton, Rev. Sci. Instrum. $\underline{55}$, 503 (1984).

14) L.D. Horton and R.M. Gilgenbach, Appl. Phys. Lett. $\underline{43}$, 1010 (1983).

15) J. VonNeumann and R.D. Richtmyer, J. Appl. Phys. $\underline{21}$, 232 (1950).

16) J.M. Picone and J.P. Boris, Phys. Fluids $\underline{26}$, 365 (1983).

17) J.M. Picone, E.S. Oram, J.P. Boris, and T.R. Young, Proceedings of the 9th Int. Colloq. on the Dynamics of Explosions and Reactive Systems, Poitiers, France, July 3-8, 1983.

18) L.D. Horton and R.M. Gilgenbach, Phys. Fluids $\underline{25}$, 1702 (1982).

19) R.D. Richtmyer, Difference Methods for Initial-Value Problems, (Interscience Publishers Inc., New York, 1957).

20) M. Raleigh, J.R. Greig, and R.F. Fernsler, NRL Memorandum
Report No. 4556, May, 1982.

Figure Captions

Fig. 1.   (a) Experimental configuration for the waxicon focused
CO_2 laser induced gas breakdown experiment.   (b) Experimental
configuration for collinear holographic interferometry of laser
guided discharges.

Fig. 2.   Schlieren photographs at different times during the
evolution of a laser guided discharge.   Upper times are relative
to the guiding laser pulse, lower times to the start of the
electrical discharge.

Fig. 3.   Comparison of theory and experiment for shock positions
in waxicon focused CO_2 laser induced gas breakdowns.   Points are
experimental data and curves are code output.   ($\triangle$) = 53 J/m
available energy, ($\square$) = 91 J/m, (o) = 105 J/m, ($\Diamond$) = 180 J/m; dot-
dashed curve= 10 J/m absorbed energy, long dashed curve= 30 J/m,
short dashed curve= 50 J/m, solid curve= 70 J/m.

Fig. 4.   Collinear holographic interferogram for a 6 cm helium
laser guided discharge channel 31 μs after discharge initiation.

Fig. 5.   Density profiles for 6 cm helium laser guided
discharges.   Points are experimental data and curves are one
dimensional hydrodynamics code results.   (a) 31 μs after
discharge, (b) 51 μs, (c) 71 μs.

Fig. 6.   Pressure profile for a 6 cm laser guided discharge
channel in helium 31 μs after discharge initiation.

11

TEA CO2 LASER

9.8cm
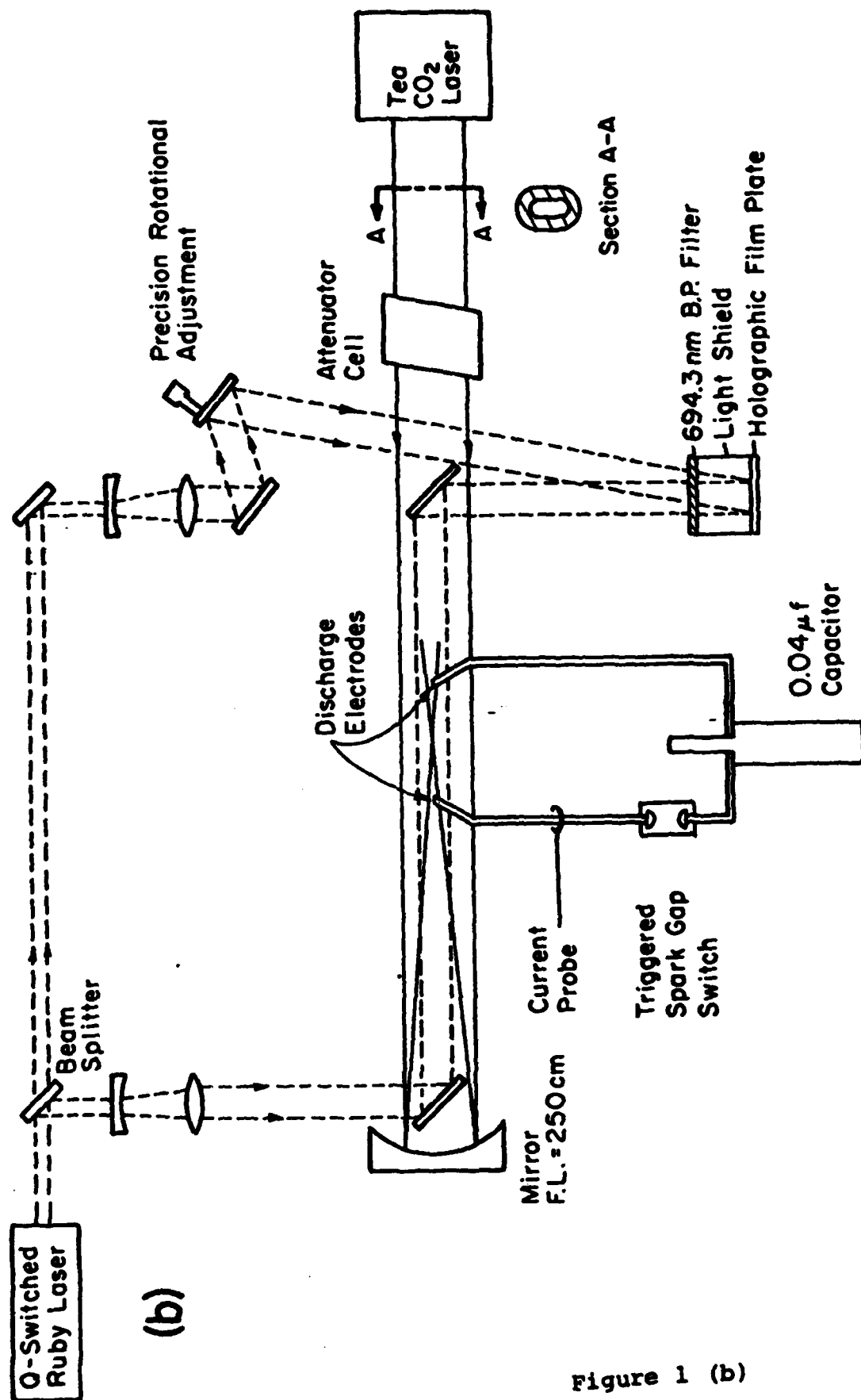
SECTION A-A

ATTENUATOR CELL

MYLAR PELLICLE WINDOW

GAS INLET

GAS OUTLET

LUCITE CHAMBER

(a)

Figure 1 (a)

Tea CO₂ Laser

Precision Rotational Adjustment

Attenuator Cell

Section A-A

694.3 nm B.P. Filter
Light Shield
Holographic Film Plate

Discharge Electrodes

0.04 μf Capacitor

Current Probe

Triggered Spark Gap Switch

Beam Splitter

Mirror F.L. = 250 cm

Q-Switched Ruby Laser

(b)

Figure 1 (b)

7.7 μs
0.1

8.7 μs
1.1

12.7μs
5.1

38.6μs
31
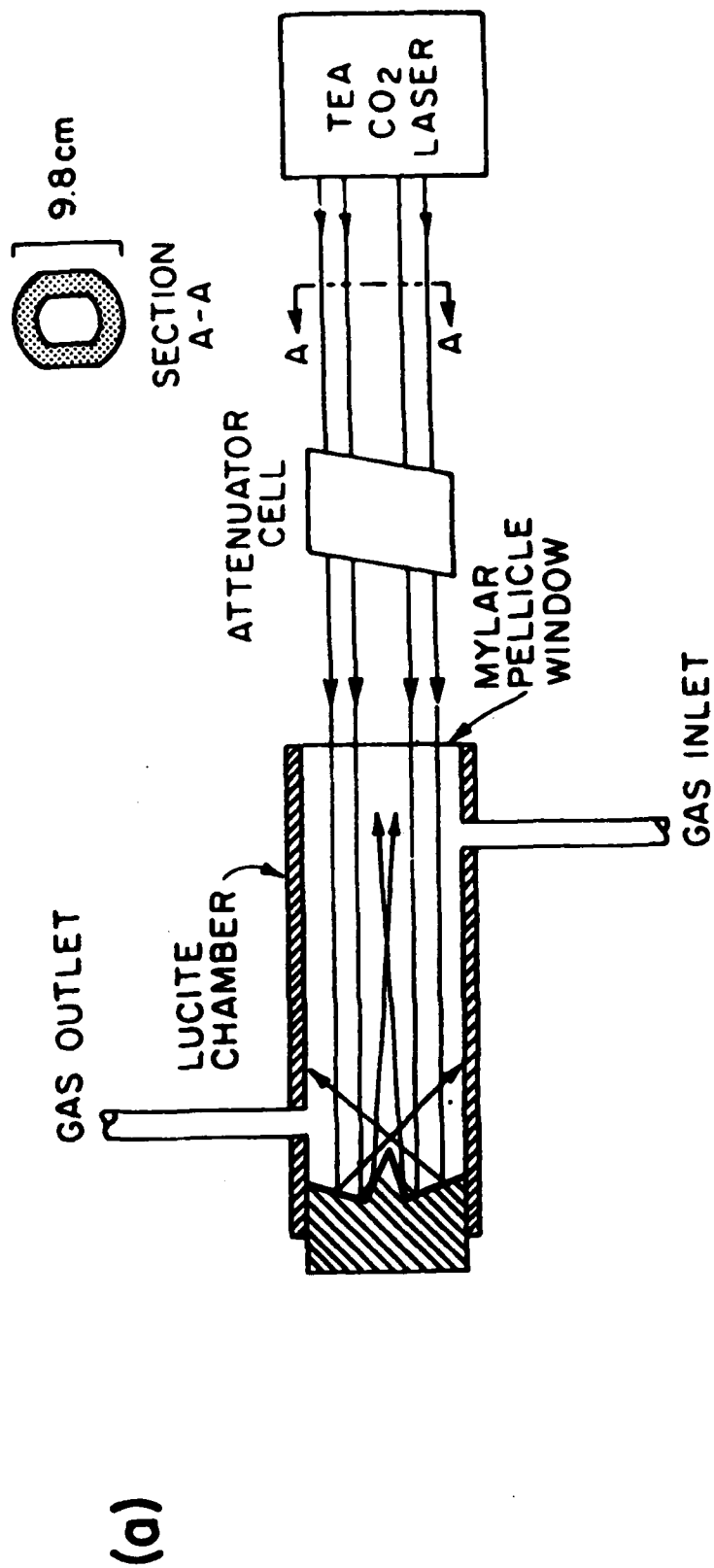
58.6μs
51
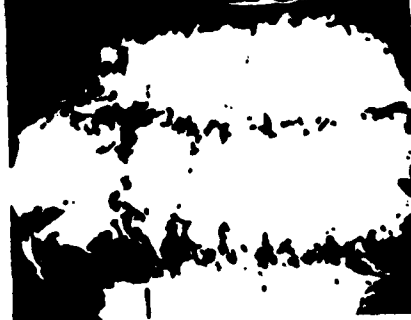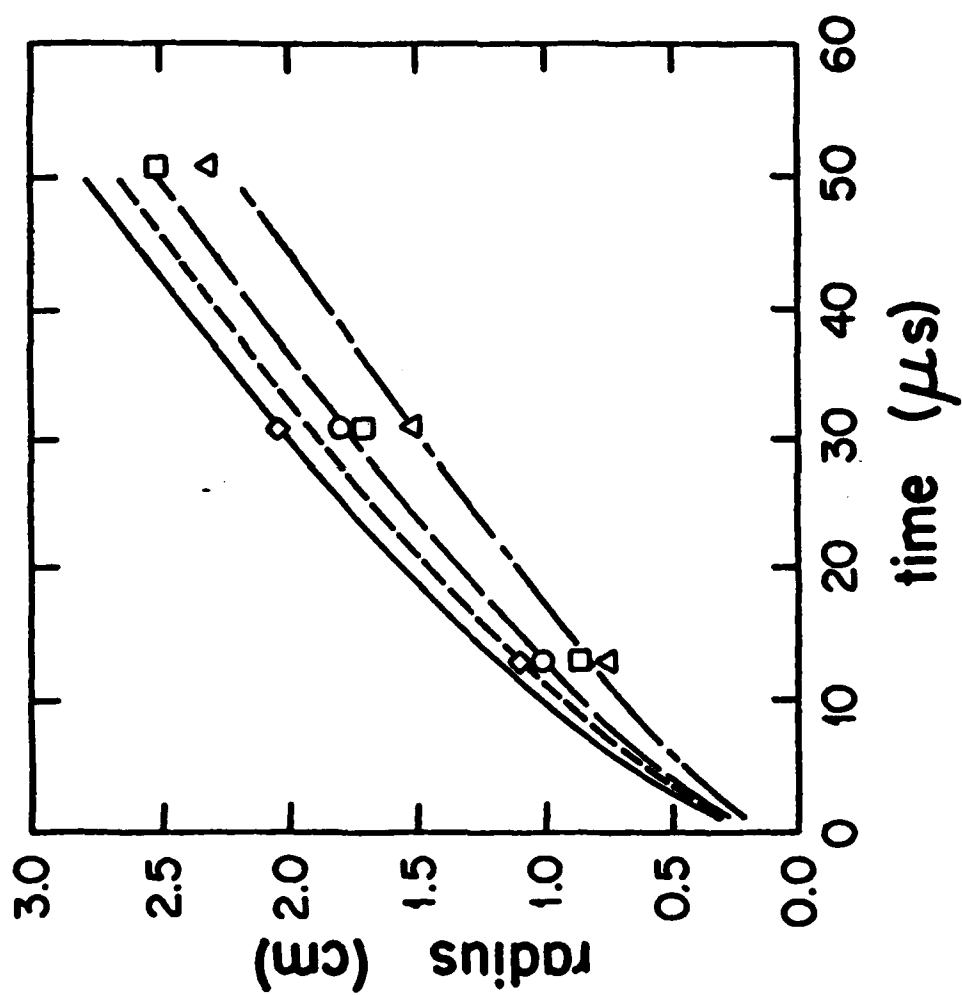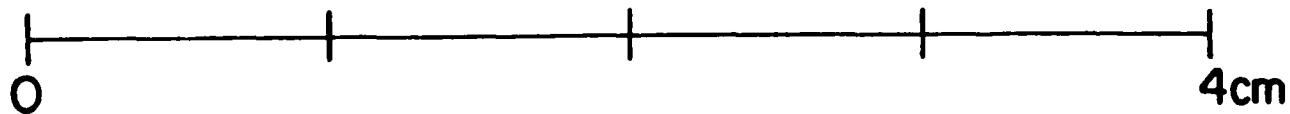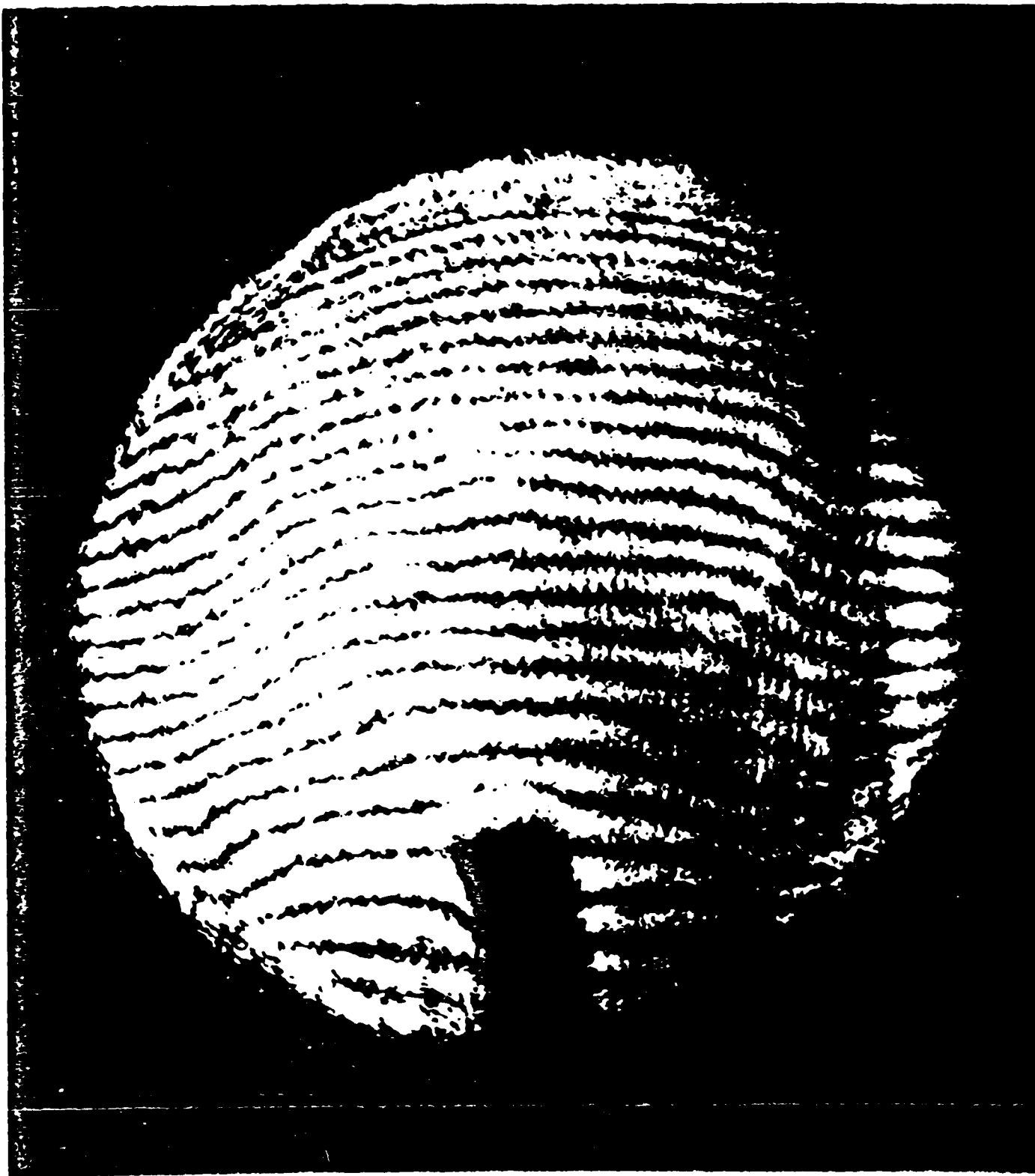
Figure 2

Figure 3

Figure 4
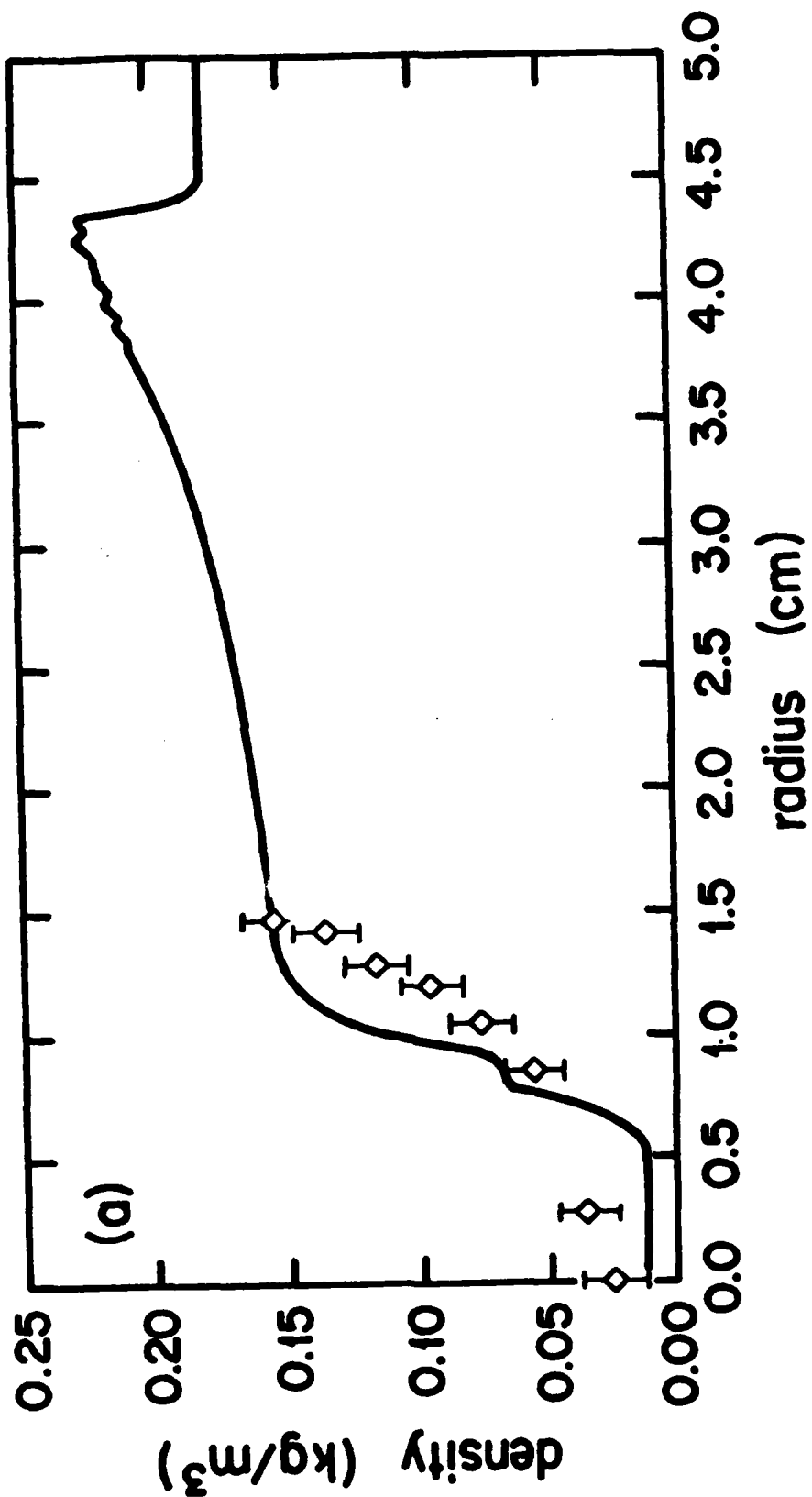
Figure 5 (a)
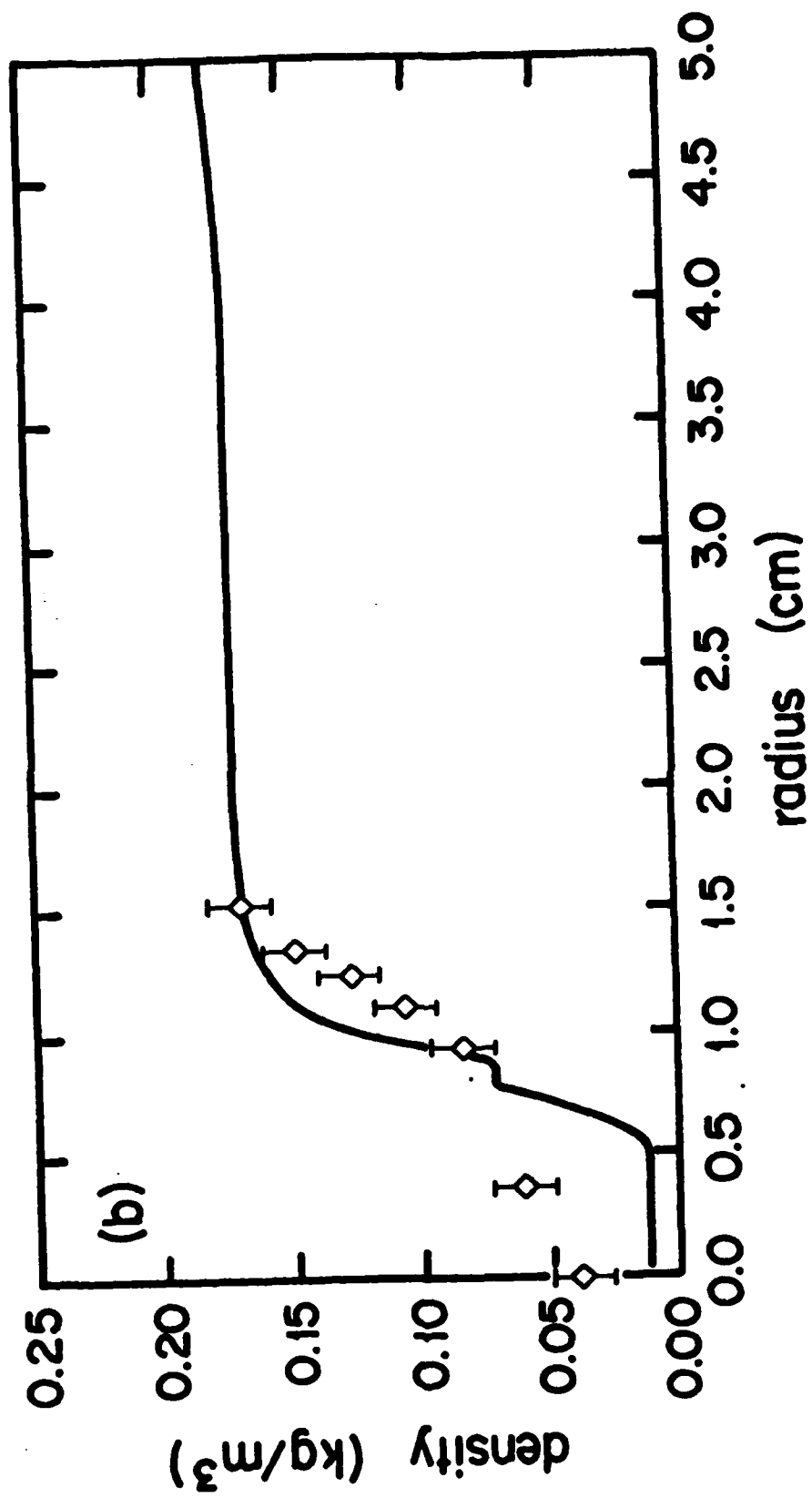
Figure 5 (b)
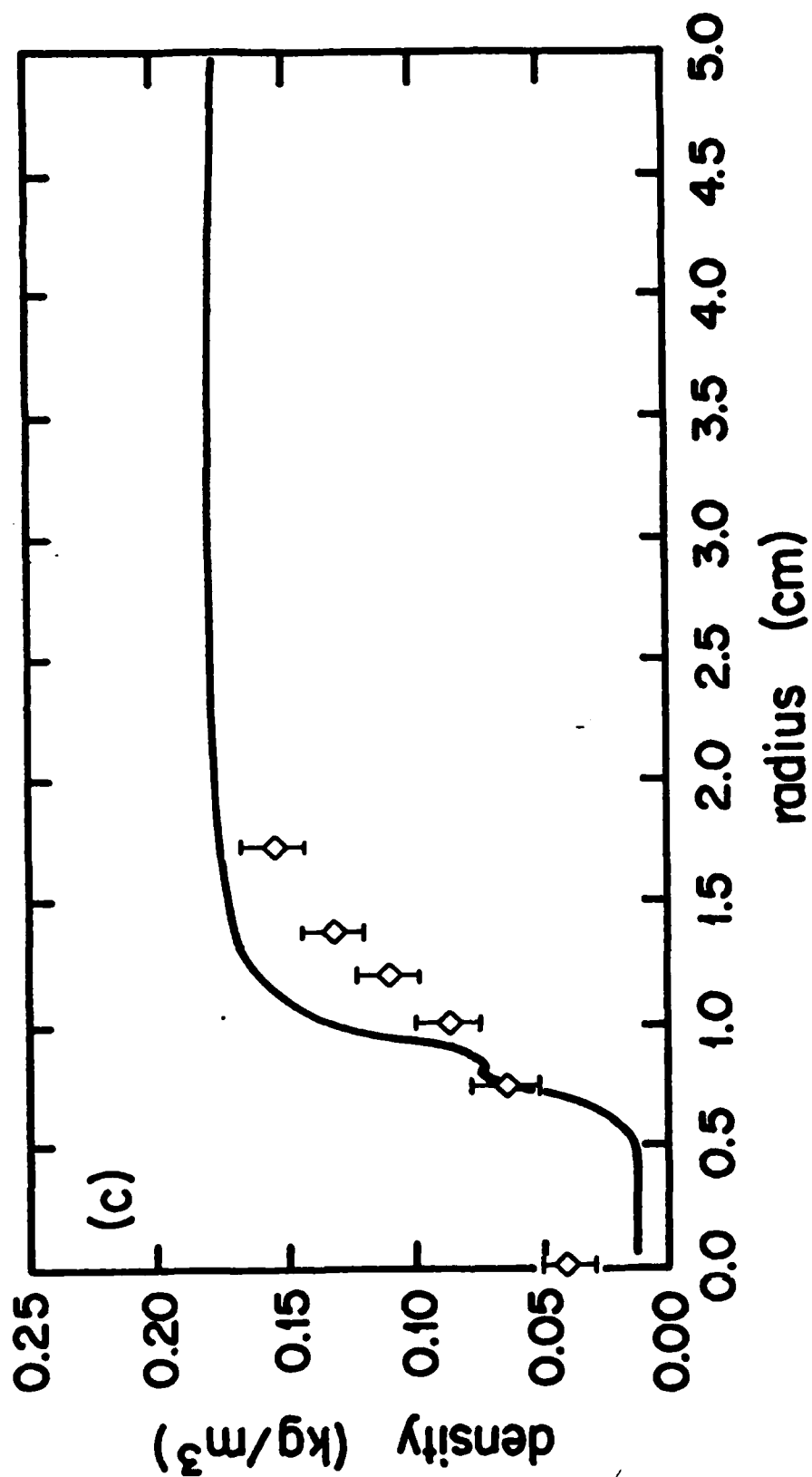
Figure 5 (c)
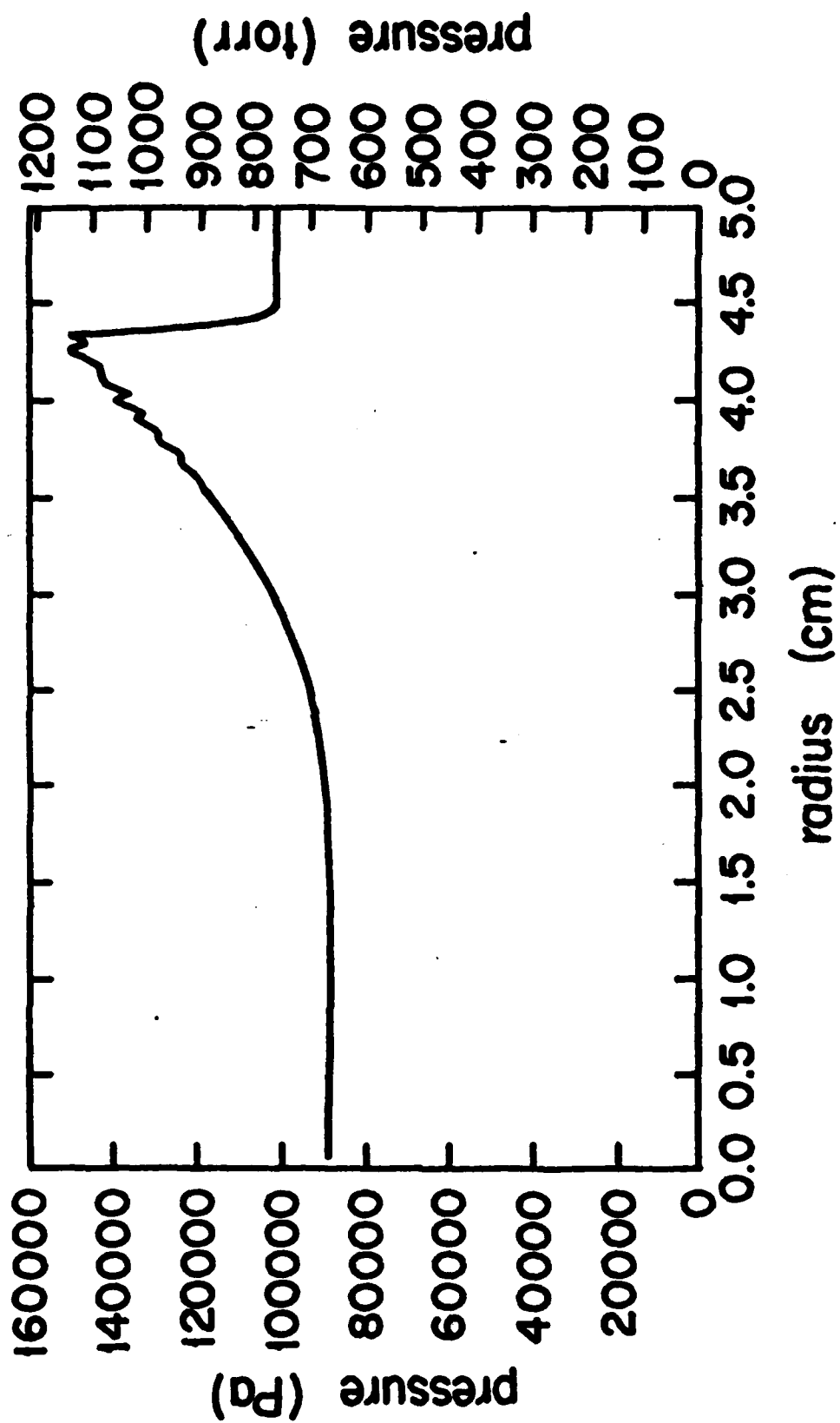
Figure 6
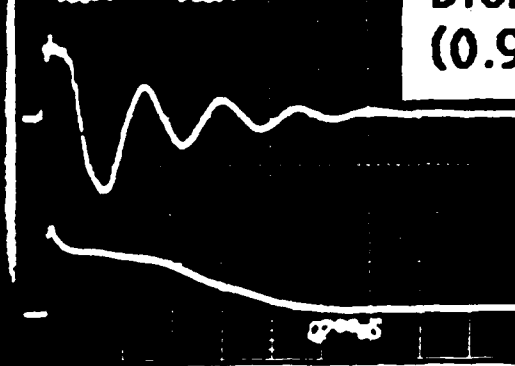
Fig. I-4

CURRENT SUSTAINMENT DATA
(0.5 MICROSEC./DIV)

ARGON DATA (2 TORR)

DIODE E-BEAM CURRENT
(0.9 kA/DIV)

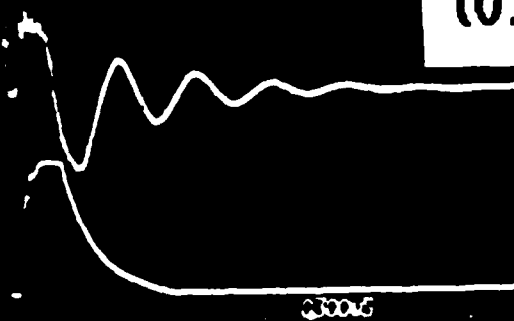COLLECTOR CURRENT
(0.4 kA/DIV)

NITROGEN DATA (2 TORR)

DIODE E-BEAM CURRENT
(0.9 kA/DIV)

COLLECTOR CURRENT
(0.4 kA/DIV)

COMPARISON OF THE L/R DECAY TIMES FOR
THE TWO GASES INDICATE THAT THE
POST-BEAM RESIDUAL RESISTIVITY OF
NITROGEN PLASMA CHANNELS IS AT LEAST A

END

FILMED

10-85

DTIC